
Fiesta: Fiber Generation and Bundle Segmentation in Tractography Using Autoencoders

Félix Dumais

Sherbrooke Connectivity Imaging Lab (SCIL)
 Videos & Images Theory and Analytics Lab (VITAL)
 Department of Computer Science
 Université de Sherbrooke, Canada
 felix.dumais@usherbrooke.ca

Jon Haitz Legarreta

Sherbrooke Connectivity Imaging Lab (SCIL)
 Videos & Images Theory and Analytics Lab (VITAL)
 Department of Computer Science
 Université de Sherbrooke, Canada

Carl Lemaire

Centre de Calcul Scientifique
 Université de Sherbrooke, Canada

Philippe Poulin

Sherbrooke Connectivity Imaging Lab (SCIL)
 Videos & Images Theory and Analytics Lab (VITAL)
 Department of Computer Science
 Université de Sherbrooke, Canada

François Rheault

Medical Imaging and Neuroinformatic (MINi) Lab
 Department of Computer Science
 Université de Sherbrooke, Canada

Laurent Petit

Groupe d’Imagerie Neurofonctionnelle (GIN)
 CNRS, CEA, IMN, GIN, UMR 5293, F-33000 Bordeaux
 Université de Bordeaux, France

Maxime Descoteaux*

Sherbrooke Connectivity Imaging Lab (SCIL)
 Department of Computer Science
 Université de Sherbrooke, Canada

Pierre-Marc Jodoin*

Videos & Images Theory and Analytics Lab (VITAL)
 Department of Computer Science
 Université de Sherbrooke, Canada

*Co-senior author. These authors contributed equally.

ABSTRACT

White matter bundle segmentation is a cornerstone of modern tractography to study the brain’s structural connectivity in domains such as neurological disorders, neurosurgery, and aging. In this study, we present FIESTA (*FIber gEneration and bundle Segmentation in Tractography using Autoencoders*), a reliable and robust, fully automated, and easily semi-automatically calibrated pipeline based on deep autoencoders that can dissect and fully populate WM bundles. Our framework allows the transition from one anatomical bundle definition to another with marginal calibrating time. This pipeline is built upon FINTA, CINTA, and GESTA methods that demonstrated how autoencoders can be used successfully for streamline filtering, bundling, and streamline generation in tractography. Our proposed method improves bundling coverage by recovering hard-to-track bundles with generative sampling through the latent space seeding of the subject bundle and the atlas bundle. A latent space of streamlines is learned using autoencoder-based modeling combined with contrastive learning. Using an atlas of bundles in standard space (MNI), our proposed method segments new tractograms using the autoencoder latent distance between each tractogram streamline and its closest neighbor bundle in the atlas of bundles. Intra-subject bundle reliability is improved by recovering hard-to-track streamlines, using the autoencoder to generate new streamlines that increase each bundle’s spatial coverage while remaining anatomically meaningful. Results show that our method is more reliable than state-of-the-art automated virtual dissection methods such as *RecoBundles*, *RecoBundlesX*, *TractSeg*, *White Matter Analysis* and *XTRACT*. Overall, these results show that our framework improves the practicality and usability of current state-of-the-art bundling framework.

Keywords Fiber Tractography · Bundling · Autoencoder · Representation Learning · Generative Sampling · dMRI

1 Introduction

White matter (WM) fiber tractography is a well-established method for brain connectivity analysis. It is currently the only non-invasive method able to investigate brain WM pathways *in vivo*. By using the local water diffusion information from diffusion-weighted Magnetic Resonance Imaging (dMRI) images, one can infer the local orientation of the underlying WM streamlines [1, 2, 3] and use it to numerically reconstruct WM pathways. Over the years, many challenges have been tackled to improve this modeling technique such as *Global Tractography* [4, 5, 6], *Probabilistic Tractography* [1, 7, 8], *Particle Filtering Tractography* (PFT) [9], *Bundle-Specific Tractography* [10, 11], or *Surface-Enhanced Tractography* (SET) [12].

The usability of WM tractography often comes from one's ability to filter and group streamlines into WM bundles. In this work, we will refer to **filtering** as any method able to remove implausible streamlines from whole-brain tractograms (filtering methods yield implausible-free whole-brain tractograms). Furthermore, there exists automated grouping methods that are 100% data-driven, fully unsupervised, whilst other methods follow pre-defined anatomical definitions. Thus, unsupervised grouping methods will be referred to as **clustering** (clustering methods yield streamline clusters), whilst grouping methods following pre-defined anatomical definitions will be referred to as **bundling** or **segmenting** interchangeably (segmenting methods yield streamline bundles). The most faithful way to extract WM bundles from a tractogram is by asking a neuroanatomist to manually dissect bundles of interest (BOI). Manual dissection of bundles is long and tedious, and is prone to large inter- and intra-expert variability [13, 14]. Automated methods, such as *QuickBundles* (QB) [15], *QuickBundlesX* (QBx) [16], *Deep Fiber Clustering* (DFC) [17, 18], *RecoBundles* (RB) [19], *RecoBundlesX* (RBx) [20], *TractSeg* [10, 21, 22, 23], *XTRACT* [24], and *White Matter Analysis* (WMA) [25, 26, 27], amongst others, have been proposed to accelerate and increase the reproducibility of this process.

Unfortunately, these grouping methods are not void of limitations. First, clustering methods are fully unsupervised, thus excluding prior knowledge of each WM bundle's class membership (*QuickBundles*, *QuickBundlesX*, DFC). Second, even if there is still a lack of consensus in the community over each bundle's anatomical definition [28], some state-of-the-art methods do not allow an easy modification of anatomical definitions (*TractSeg*, *XTRACT*). In fact, if a change in bundle definitions is needed with *TractSeg* [21], a full reannotation of the training dataset is required alongside with a complete retraining of its three neural networks. Contrastingly, *XTRACT* [24] heavily relies on regions of interest (ROI) drawn by expert neuroanatomists to work properly. Those ROIs are usually hard to get and prone to inter-expert variability. Third, methods such as WMA are impractical in a large scale context because they rely on an affinity matrix computed using the pairwise distance of each streamline in a whole-brain tractogram. Such methods have prohibitive memory usage when the tractogram has more than 500,000 streamlines [21]. Fourth, methods such as *RecoBundles* [19] and *RecoBundlesX* [20] require the non-trivial calibration of several parameters and are more or less reliable in a test-retest analysis (see *RecoBundles* and *RecoBundlesX* results in section 3). Finally, knowing all the limitations of dMRI tractography [28], bundling and clustering methods are tied to the tracking algorithms' ability to recover hard-to-track WM bundles in the first place.

In this paper, we present FIESTA (*FIber gEneration and bundle Segmentation in Tractography using Autoencoders*), a reliable and robust, fully automated, and easily semi-automatically calibrated pipeline based on deep autoencoders that can dissect and fully populate WM bundles. FIESTA allows an easy change in its bundle definitions, depending on the need, with a marginal calibrating time. This pipeline is built upon FINTA, CINTA, and GESTA methods [29, 30, 31] that demonstrated how autoencoders can be used successfully for filtering, bundling, and streamline generation in tractography.

1.1 Related work

Over the years, many methods have been developed to ease the interpretability of whole-brain tractograms, such as filtering methods [29, 32, 33, 34, 35] and clustering methods [15, 16, 17, 18, 25, 36, 37]. Unfortunately, filtering methods do not allow to easily target anatomical regions as tractograms are not grouped in streamline bundles. On the other hand, streamline clustering algorithms, a class of methods designed to group streamlines with similar properties, are typically built upon unsupervised machine learning approaches such as mixture models, spectral clustering and hierarchical clustering. Unfortunately, clustering methods suffer from a major drawback: they offer no control to which cluster belongs to which WM anatomical region.

Therefore, bundling comes as a solution for this problem. It aims to give streamlines an anatomical label. Many methods have been proposed in the literature to bundle whole-brain tractograms, such as TRACULA [38], *TractQuerier* [39], or *Classifyber* [40]. In this work, we will confine our reference methods to *RecoBundles* [19] and *RecoBundlesX* [20], WMA [25, 26, 27], *TractSeg* [10, 21, 22, 23] and *XTRACT* [24]. Reference methods for this work were based on different criteria. The main goal was to capture the representativeness of the different existing state-of-the-art methods. *RecoBundles* and *RecoBundlesX* were selected for their ease of implementation, and because author F.R. developed the

latter. *XTRACT* was selected to represent ROI-based bundling methods. WMA was selected to represent methods based on a non-physical embedding space. Finally, *TractSeg* was selected to capture the effectiveness of supervised deep learning methods.

RecoBundles is a well-established method based upon atlas bundles pre-segmented by medical experts. When a new tractogram needs to be bundled, a streamline-based linear registration [41] is done between the target and the atlas tractograms, bringing the tractogram and the atlas in the same space. After this co-registration, a sequence of operations is performed for each bundle in the atlas. First, the target tractogram is pruned to remove irrelevant streamlines to the current bundle of interest. Then, a local streamline-based linear registration is performed to better match the target anatomy. Finally, a second pruning operation is performed using a stricter distance threshold to isolate the streamlines that have a high shape similarity to the current bundle of interest in the atlas. All the aforementioned steps are performed using centroids rather than individual streamlines to speed up processing.

RecoBundlesX is an improved version of *RecoBundles* using many iterations of *RecoBundles* over multiple atlases with different sets of parameters. Varying parameters are (i) whole-brain tractograms *QuickBundles* clustering thresholds, (ii) atlas bundle *QuickBundles* clustering thresholds, and (iii) pruning thresholds. While being much more reliable than *RecoBundles*, this method is time-consuming since *RecoBundles* is launched many times.

White Matter Analysis (WMA), proposed by O’Donnell, L. *et al.*, (2007) [25], is an atlas-based bundle recognition method where streamline classification is done in an embedding space built with spectral clustering [42, 43]. The atlas streamlines are represented as a point in the embedding space, where each point is assigned to a bundle class. New tractogram streamlines are bundled using the closest atlas centroid as the most probable class. One drawback of the method is that it requires computing an $N \times N$ pairwise streamline distance affinity matrix, which is computationally prohibitive for a reasonably sized tractogram. Therefore, the Nystrom approximation [44] is done as a trade-off to approximate the affinity matrix.

XTRACT [24] is a bundling method built upon an atlas of ROIs. ROIs are defined in a standard space and contain starting areas, inclusion and exclusion zones, and termination areas for each bundle. The regions are non-linearly registered to the diffusion space and used to bundle raw tractograms.

TractSeg is a state-of-the-art deep learning bundling method. Presented over many articles [10, 21, 22, 23], the latest version works in three steps. First, a constrained spherical deconvolution (CSD) is used over the diffusion orientation distribution function (dODF) to extract the three principal peaks from the obtained fiber orientation distribution function (fODF). Next, peak maps are given to three U-Net neural networks (NN) [45] yielding $B = 72$ bundle segmentation maps, $2 \times B$ start and end bundle segmentation maps, and B bundle-specific *Tract Orientation Maps* (TOM). Finally, probabilistic tractography is done over each TOM within their respective bundle segmentation maps and making sure start and end regions are respected for each streamline.

1.2 Contributions

In this paper, we present a semi-supervised bundling method called *FIESTA*. This work is the natural extension of FINTA [29], CINTA [30], and GESTA [31], which use a deep convolutional autoencoder to project streamlines into a lower, more structured, smoother and locally linear dimensional space to either filter, segment, or generate WM streamlines. To better structure the latent representation, we trained the autoencoder with a contrastive loss [46] informed by *QuickBundlesX* clustering. *FIESTA* uses an autoencoder to filter and bundle whole-brain tractograms based on a given bundle atlas. It also takes advantage of its latent space sampling strategy to synthesize new streamlines and improve the coverage of its bundles. To avoid confusion and to be sure to distinguish the slight method variations between previous works and the current implemented methods, we will rename the implemented 2-in-1 filtering and bundling method as *FIESTA-seg*, and the implemented generative method as *FIESTA-gen* (c.f. section 2). Thus, this work makes the following five contributions:

1. *FIESTA* leverages the power of previous fiber autoencoders [29, 30, 31] and overcomes their individual limitations, yielding a pipeline able to work adequately in an end-to-end *in vivo* dMRI data analysis scenario;
2. *FIESTA* is more reliable than current state-of-the-art automatic bundling methods;
3. We show that the usage of generative sampling improves the bundle-wise volumetric reliability;
4. We show that we can train and use contrastive learning based on *QuickBundlesX* clusters to build a useful latent representation of a whole-brain tractogram;
5. Bundle definitions are easily editable in *FIESTA* without the need to re-train a neural network.

2 Methods

FIESTA's three main underlying key concepts are summarized in Fig. 1. First, an autoencoder is used to learn a streamline representation latent space (c.f. Fig. 1a). Next, given a new tractogram and a reference set of bundles (typically provided by a trained specialist), FIESTA-seg extracts false-positive-free bundles from a given whole-brain tractogram (c.f. Fig. 1b). Finally, FIESTA-gen populates each bundle by generating plausible streamlines supported by a filtering process to increase the spatial coverage (Fig. 1c)¹. FIESTA is a software suite built upon previous works that yields WM bundles from the concatenation of the output bundles of FIESTA-seg and FIESTA-gen.

2.1 Data

Three datasets were used for the development and the testing of FIESTA – namely *TractoInferno* [48], and the Human Connectome Project (HCP) [49, 50] as shown in Fig. 1, and *MyeloInferno* [51] for the evaluation. The choice of datasets was based on several criteria, such as ease of access, multiple time-points per subject (*MyeloInferno*), high quality data (HCP), and the availability of multiple WM tracking types (*TractoInferno*). *TractoInferno* and HCP data were used for the training of the convolutional autoencoder and early evaluation stage, while *MyeloInferno* was employed to evaluate the reliability of the pipeline. Also, *TractoInferno* ‘silver standard’ [52] bundles were used for the threshold calibration steps. HCP subjects were also used for adjusting FIESTA-gen’s parameters.

TractoInferno [48] is a publicly available, widely heterogeneous database designed for machine learning purposes in dMRI tractography. It is composed of 354 subjects from 6 different datasets acquired with 5 different MRI scanners with various image resolutions, acquisition parameters, and subject ages. MRI acquisitions underwent a manual quality control (QC) process before using an ensemble of four tracking types – namely local deterministic, local probabilistic, PFT [9], and SET [12] – before being processed into *RecoBundlesX*, yielding its silver standard.

MyeloInferno [51] is a non-public dMRI dataset composed of 20 young and healthy subjects (mean age 36 years \pm 4.7 [standard deviation]; 17 women). Written informed consent was obtained from participants and were recruited following the ethics protocol of the Centre de Recherche du Centre Hospitalier Universitaire de Sherbrooke. The data includes 5 acquisitions for each subject. Thus, the data are ideal to evaluate the reproducibility of our pipeline. All images were acquired on a 3T Ingenia MR scanner with a 32-channel head coil (Philips Healthcare, Best, Netherlands) with T1w images acquired with a resolution of 1 mm isotropic voxels and dMRI images acquired with a resolution of 2 mm isotropic voxels, 100 gradient directions uniformly distributed over three shells ($b = \{300(8), 2000(32), 3000(60)\} \text{ s/mm}^2$) (the number of directions per shell is in parentheses), and 7 unweighted images. After a manual QC of the dataset, 18 subjects (with 5 acquisitions each) were kept, yielding 90 whole-brain tractograms. Each tractogram was an ensemble of tractograms generated using the *TractoFlow* pipeline [53], which provided a PFT probabilistic tracking and a local probabilistic tracking that were concatenated. PFT tractograms were generated using interface seeding with 30 seeds per voxel, while local tractograms were generated using white matter seeding with 10 seeds per voxel. Both tracking methods were constrained with a streamline length range between 20 and 200 mm.

The Human Connectome Project Young Adult dataset [49, 50] is a dataset of approximately 1200 subjects (age range 22-35 y/o) composed of different MRI modalities. For the purposes of this project, only the T1w and dMRI acquisitions were used. All images were acquired on a 3T MR scanner with T1w images acquired with a resolution of 0.7 mm isotropic voxels and dMRI images acquired with a resolution of 1.25 mm isotropic voxels, 270 gradient directions equally distributed over three shells ($b = \{1000, 2000, 3000\} \text{ s/mm}^2$) and 6 unweighted images. Again, the tracking was done using the *TractoFlow* pipeline [53] based on fODF estimated using $b = \{0, 1000, 2000, 3000\} \text{ s/mm}^2$ shells, which provided a PFT probabilistic tracking and a local probabilistic tracking that were concatenated. PFT tractograms were generated using interface seeding with 60 seeds per voxel, while local tractograms were generated using white matter seeding with 30 seeds per voxel. Both tracking methods were constrained with a streamline length range between 20 and 200 mm.

TractoFlow [53] was used to process HCP and *MyeloInferno* subjects, yielding PFT and local probabilistic whole-brain tractograms, while *TractoInferno* authors were reached to get access to original raw tractograms (PFT, SET [12], local deterministic tracking and local probabilistic tracking).

2.1.1 Bundle Atlas

As shown in Fig. 1, standard space ideal bundles (i.e., an atlas) are needed as a reference for FIESTA to work properly. For the development and the evaluation of the current pipeline, we used an in-house and publicly available Population Average of WM (PAWM) atlas to evaluate our framework [54]. The PAWM atlas was built in the context of

¹FIESTA-seg: ‘seg’ for tractogram Segmentation; FIESTA-gen: ‘gen’ for streamline Generation.

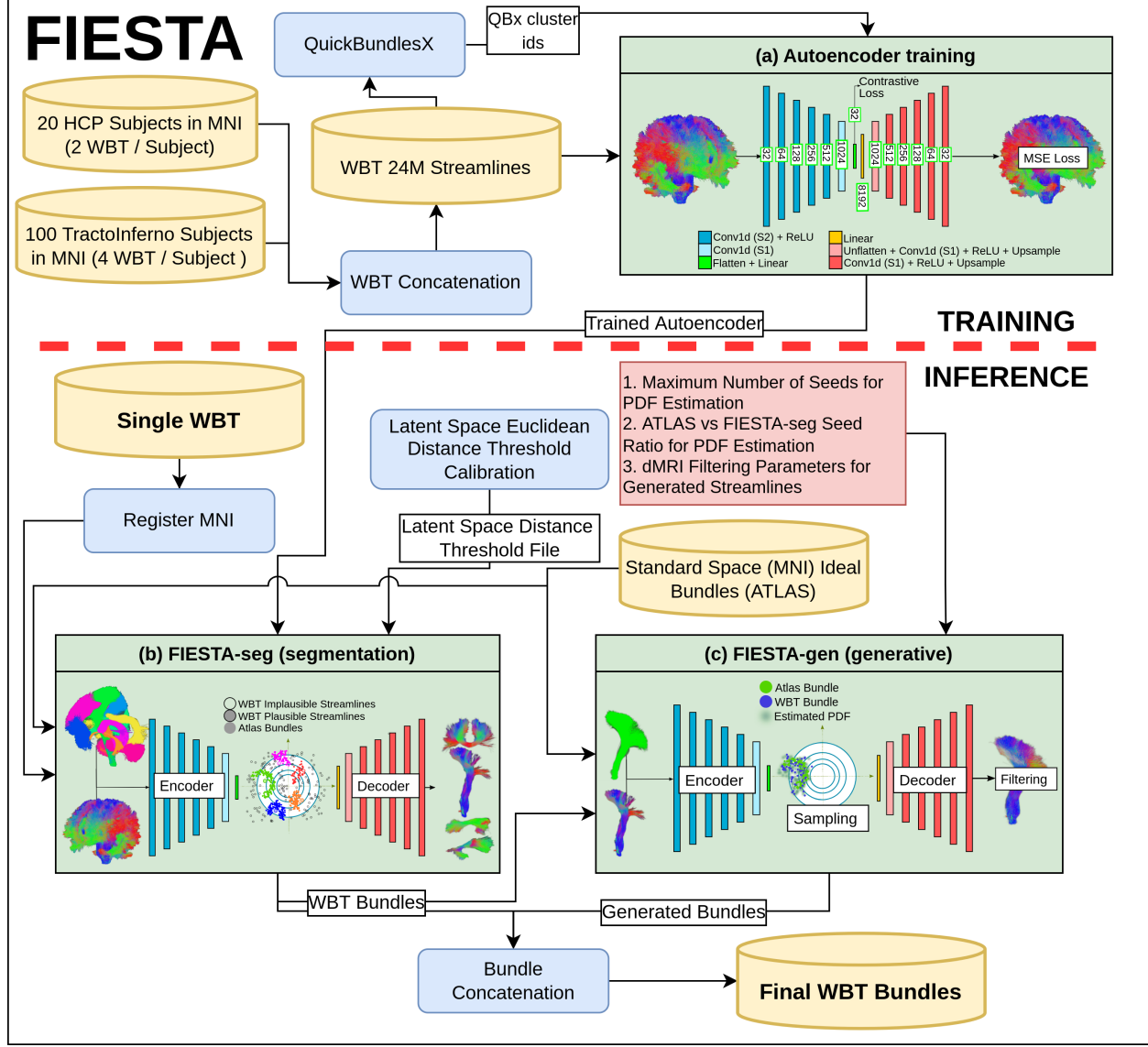


Figure 1: FIESTA pipeline. (a) Training of a convolutional autoencoder on raw dMRI whole-brain tractograms (WBT) with a combination of a mean squared error (MSE) loss and a contrastive loss. A streamline is a 1D signal with 3 channels. The contrastive loss' positive and negative pairs are based on *QuickBundlesX* streamline cluster memberships, (b) The trained autoencoder is used to filter and bundle streamlines based on a k-nearest neighbors algorithm and a Euclidean distance threshold. The key idea behind the autoencoder's latent space is that plausible streamlines fall closer to the cleaned, filtered, and averaged bundles in the standard atlas than implausible streamlines, (c) A probability distribution function (PDF) is empirically estimated with a Parzen estimator [47] based on the embedding of each bundle and its atlas counterpart. Rejection sampling is used to generate new streamline samples from the estimated PDF. Sampled streamlines are then filtered by checking their fit to the underlying diffusion signal, a length range, a maximum winding angle, and a WM coverage rate, finally yielding a bundle with better spatial coverage.

RecoBundlesX works by Rheault, F. *et al.*, (2020) [19, 20] based on ExTractor [55] and well-curated by a neuroanatomist to finally have bundles that fit their normative shapes [54]. Fig. 2 presents a representation of all the bundles in the PAWM atlas. Full names, abbreviations, and labels of bundles used in this work are indicated in Supplemental section A.1, whilst more context on the method used to generate these bundles is given in Supplemental section A.5.

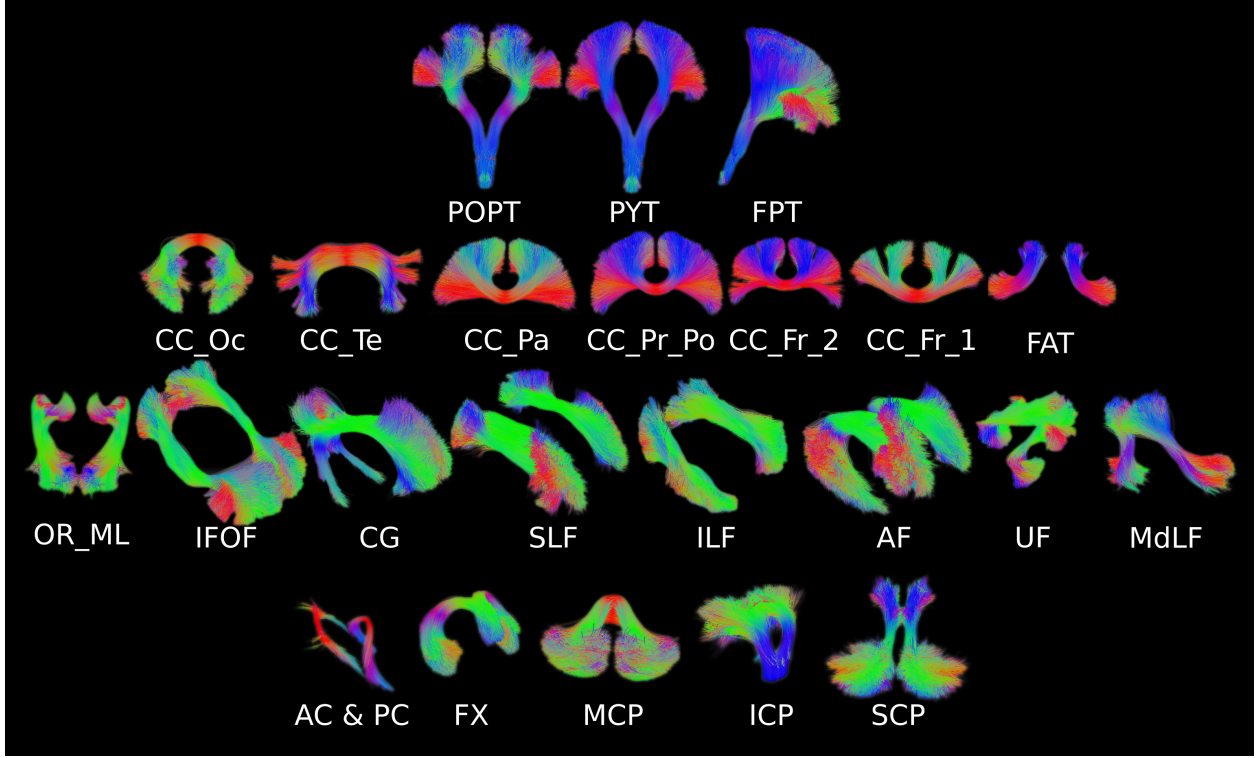


Figure 2: PAWM atlas bundles used for FIESTA development and evaluation. All symmetric bundles are joined together (left and right). Abbreviations are described in full detail in section A.1.

2.2 Tractogram embedding

Fig. 1a shows a summary of the autoencoder’s embedding and training scheme of the whole human brain streamlines. Autoencoders [56] are a type of neural network designed to compress and reconstruct input data as faithfully as possible. They are made of an encoder (in blue) and a decoder (in red), two 1D convolutional neural networks in our case. The encoder projects a sample from the input space to a latent space, and the decoder reverses that operation. An undercomplete autoencoder [57] is one whose latent representation dimensionality is smaller than that of the input data. This forces the autoencoder to learn a latent space which embeds the most salient features of the input data. A well-constructed autoencoder encodes streamlines with similar properties (i.e., shapes, anatomical location, etc.) close to each other in the latent space.

Let $\mathcal{S} = \{S_1, \dots, S_N\}$ be a set of N streamlines registered in a common space (e.g., MNI [58, 59] for the current pipeline) with $S_i = [\mathbf{s}_i^1, \dots, \mathbf{s}_i^k]$ where k is the number of vertices per streamline and $\mathbf{s}_i^j \in \mathbb{R}^3$. By making sure that $k = D$ for all streamlines, with D being a constant, we train a 1D convolutional autoencoder on raw whole-brain tractograms to learn a useful WM streamline latent representation. The training loss contains two terms: an MSE reconstruction loss and a contrastive loss to help the bundling problem.

The contrastive loss runs over pairs of samples S_i, S_j to enforce streamlines of the same bundle to be as close as possible in the latent space. Following Hadsell, R. *et al.*, (2006) [46], the contrastive loss is built upon a binary label y where $y = 0$ if S_i and S_j have similar properties and $y = 1$, if S_i and S_j are dissimilar. Also, let the parameterized Euclidean distance between two streamlines be defined as

$$D_\theta(S_i, S_j) = \|p_\theta(S_i) - p_\theta(S_j)\|_2, \quad (1)$$

where p_θ is the encoder function. The contrastive loss function is

$$\mathcal{C}(\theta) = \sum_{i=1}^N C(\theta, y, S_i, S_j), \quad (2)$$

with

$$C(\theta, y, S_i, S_j) = (1 - y)C_S(D_\theta) + yC_D(D_\theta). \quad (3)$$

C_S and C_D are designed such that minimizing C w.r.t θ would result in low values of D_θ when S_i, S_j are within the same bundle and high values for D_θ otherwise. Therefore,

$$C(\theta, y, S_i, S_j) = (1 - y) \frac{1}{2} (D_\theta)^2 + y \frac{1}{2} \{ \max(0, m - D_\theta) \}^2, \quad (4)$$

where the contrastive loss margin was set to $m = 1.25$, as in Hadsell, R. *et al.*, (2006) [46].

Since whole-brain tractograms come with no annotation, similar and dissimilar pairs of streamlines are determined based on *QuickBundlesX* clusters [16] obtained with $\{40, 30, 20, 10\}$ mm as input parameters. Thus, similar (or positive) streamline pairs are taken from the same *QuickBundlesX* cluster, whilst dissimilar (or negative) streamline pairs are taken from two different clusters.

Finally, the MSE reconstruction loss is defined as

$$\mathcal{M}(\theta, \phi) = \sum_{i=1}^N \|\hat{S}_i - S_i\|_2^2, \quad (5)$$

where $\hat{S}_i = q_\phi(p_\theta(S_i))$ is a reconstructed streamline and $q_\phi(\cdot)$ is the decoder. Therefore, the overall training loss is

$$\mathcal{L}(\theta, \phi) = \mathcal{M}(\theta, \phi) + \lambda \mathcal{C}(\theta), \quad (6)$$

with λ being a hyperparameter. The hyperparameter λ was empirically determined to approximately balance the MSE loss with the contrastive loss on a randomly initialized autoencoder. In our case, the optimal value was $\lambda = 400$.

2.2.1 The autoencoder training scheme

We trained the autoencoder in a train-validation-test scheme. Our whole dataset is composed of 120 subjects randomly shuffled with an 80/20 split between *TractoInferno* and HCP datasets (c.f. section 2.1). The train/validation/test split was therefore 100/10/10. 200,000 streamlines per subject were used, with 100,000 streamlines per HCP whole-brain tractogram ($N = 2$ – namely PFT and local probabilistic tracking) and 50,000 streamlines per *TractoInferno* whole-brain tractogram were randomly sampled from each raw tractograms ($N = 4$ – namely PFT, SET, local deterministic tracking and local probabilistic tracking). In total, our dataset contains 24,000,000 streamlines. Also, each streamline is resampled to a fixed dimensionality of $D = 256$ 3D vertices and the latent space dimensionality is fixed to $d = 32$.

2.3 Tractogram Segmentation

Once the autoencoder is trained, one can use it to filter and bundle a new tractogram. As displayed in Fig. 1b, every streamline that ought to be filtered and segmented is registered into the MNI reference space and projected into the latent space using the encoder neural network. This is done alongside the bundle streamlines of the atlas. A k-nearest neighbors (k-NN) algorithm is used to assign each streamline (in the latent space) to the majority class label among the nearest atlas streamline (also in the latent space). The absolute Euclidean distance between the WM streamline and its atlas counterpart is then compared to a pre-determined threshold. To determine the threshold that best balances true positives and false positives, a ROC curve was used, as suggested by Legarreta, J. *et al.*, (2021) [29], alongside manual adjustment (c.f. section 2.3.1). Manual adjustments were mandatory to qualitatively match atlas bundles. Thus, if the distance is smaller than the threshold, the streamline is kept for downstream tasks. Otherwise, the streamline is considered implausible and, therefore, discarded.

2.3.1 Latent space distance threshold calibration steps

Bundling methods require a calibration to account for each bundle's unique shape; for example, with *RecoBundles* and *RecoBundlesX*, there are multiple parameters to set for each bundle. Fortunately, with FIESTA there is only one threshold per bundle (c.f. Fig. 4 to see threshold effect on bundles). For calibration, a per-bundle *optimal* threshold was determined automatically followed by manual adjustments around the *optimal* threshold to obtain the desired bundle shape (c.f. Fig. 3). *Optimal* thresholds were found by equally distributing the per-bundle true positive and false positive streamlines, using the ROC curve analysis method presented by Legarreta, J. *et al.*, (2021) [29]. We used *TractoInferno* silver standard [52] bundles in the validation set as true positive streamlines. We consider as implausible the streamlines from the raw tractogram that are absent from the silver standard bundles. The bundle-wise thresholds are thus determined as follows:

1. Encode atlas bundles and their flipped versions into latent vectors;

2. Encode plausible silver standard bundles and implausible streamlines and their flipped version from the validation set;
3. For each latent vector from the validation set (plausible and implausible), find the closest streamline in the atlas using a k-NN algorithm. This step forms groups of plausible and implausible streamlines with a class label;
4. For each group of streamlines, optimize the Euclidean distance threshold that maximizes the number of true positive streamlines and minimize the number of false positive streamlines. Note that during this stage, plausible streamlines assigned to the wrong class are considered implausible. This step is equivalent to taking the threshold value at the intersection between each ROC (bundle-wise) curve and the inverse diagonal line;
5. Qualitatively manually adjust the *optimal* thresholds, if needed, to improve atlas bundle similarity with the validation set bundles.

To understand the effect of the choice of threshold, we visually inspected the shape and the quality of the resulting bundles. We set up an experiment with a subset of the bundles from the atlas presented in section 2.1.1. We studied the effect of 8 uniformly spaced threshold values centered on the *optimal* threshold of the AF_L, the CC_Pr_Po, the IFOF_L, the OR_ML_L, the PYT_L and the UF_L bundles. Fig. 4 illustrates the results of that experiment. We set the values using 20% increments based on the ROC curves analysis thresholds. Therefore, it is possible to observe that low thresholds seems to increase bundle specificity at the expense of the sensitivity. On the other hand, high threshold values, classifying more streamlines as positives, increase the sensitivity at the expense of the bundle specificity. Red circles in Fig. 4 indicate streamlines that should not be part of final bundles based on the atlas ideal bundles. Interestingly, such streamlines are not always present when the threshold used is higher than the *optimal* threshold. In fact, we see that spurious streamlines are still present in the OR_ML even with a 40% threshold reduction. Thus, this analysis shows that threshold manual adjustment is mandatory and threshold values based only on ROC curves analysis should not all be used as is. In our case, for some bundles, we needed to decrease the latent space distance threshold, thus increasing the specificity, to more closely match, qualitatively, bundles from the PAWM atlas (c.f. Fig 2).

2.4 Bundle coverage improvement using generative sampling (Fiesta-gen)

As shown in Fig. 1c, FIESTA-gen is used, after FIESTA-seg, to better populate each bundle. This module compensates the imperfections of the latent space-based threshold segmentation method and the missing streamlines in the original whole-brain tractogram, especially in hard-to-track bundles [11]. Thus, for each bundle in the atlas, we take the clustered streamlines by FIESTA-seg for the current bundle (see Fig. 1b). An input ratio (0.5:0.5, c.f. Supplemental section A.3) between the number of streamlines to use from each bundle (atlas and FIESTA-seg output) is specified alongside the maximum total number of streamlines to use. The decision to estimate the latent space PDF with streamlines from the subject bundles and the atlas bundles was motivated by the fact that ideal bundles are built to fully cover the target anatomical region. Therefore, missing streamlines from the original bundles can be recovered if a portion of the streamline seeds [31] for the latent space PDF estimation is based on the atlas bundles. Then, all streamlines used to estimate the PDF are embedded with the encoder. The PDF is empirically estimated using a Parzen estimator [47] over all embedded points with a Gaussian kernel. The kernel bandwidth is automatically estimated using Silverman's rule of thumb [60].

As described in [31, 61], since streamline latent representations live in a locally linear manifold, rejection sampling (RS) [47] can be used to sample new data from an empirically estimated PDF. Thus, giving a set of latent vectors \mathcal{Z} with $\mathbf{z}_i \in \mathbb{R}^d$, $\mathbf{z}_i \subset \mathcal{Z}$ and $\mathbf{z}_i = p_\theta(S_i)$, our goal is to estimate a new set of latent vectors $\mathcal{Z}' \not\subset \mathcal{Z}$ where the new PDF of estimated vectors $P(\mathbf{z}')$ is close to $P(\mathbf{z})$. As described previously, the PDF of $P(\mathbf{z})$ is unknown, and we estimate it with a Parzen estimator. Because $P(\mathbf{z})$ is difficult to sample, we sample an easier PDF $Q(\mathbf{z})$. In our case, $Q(\mathbf{z})$ is a mixture of Gaussians estimated with the expectation-maximization algorithm [47]. The RS procedure works as follows: one first generate a random sample from $Q(\mathbf{z})$ as well as a random number u_0 i.i.d. of a uniform distribution between $[0, KQ(\mathbf{z})]$ where K is a constant. If $u_0 > P(\mathbf{z})$, the sample is rejected, otherwise it is accepted.

Finally, the accepted vectors are decoded to generate new streamlines. As described in GESTA [31], those streamlines need to fit certain anatomical constraints. Therefore, we adopt the four proposed constraints – namely a length range, a WM coverage, a maximum curving angle, and the local streamline orientation to fODF peak angle (c.f. Supplemental section A.2). Furthermore, we trim off the vertices at each end of generated streamlines that overshoots the gray matter with a WM mask. The final bundles used for evaluation are the concatenation of FIESTA-seg and FIESTA-gen bundles.

2.4.1 Number of generated streamlines

To assess the capacity of FIESTA-gen to generate diverse streamlines that “fill” the anatomy well, we have produced saturation curves [62, 20], which plot the bundle volume with respect to the streamline count. We expect that if adding

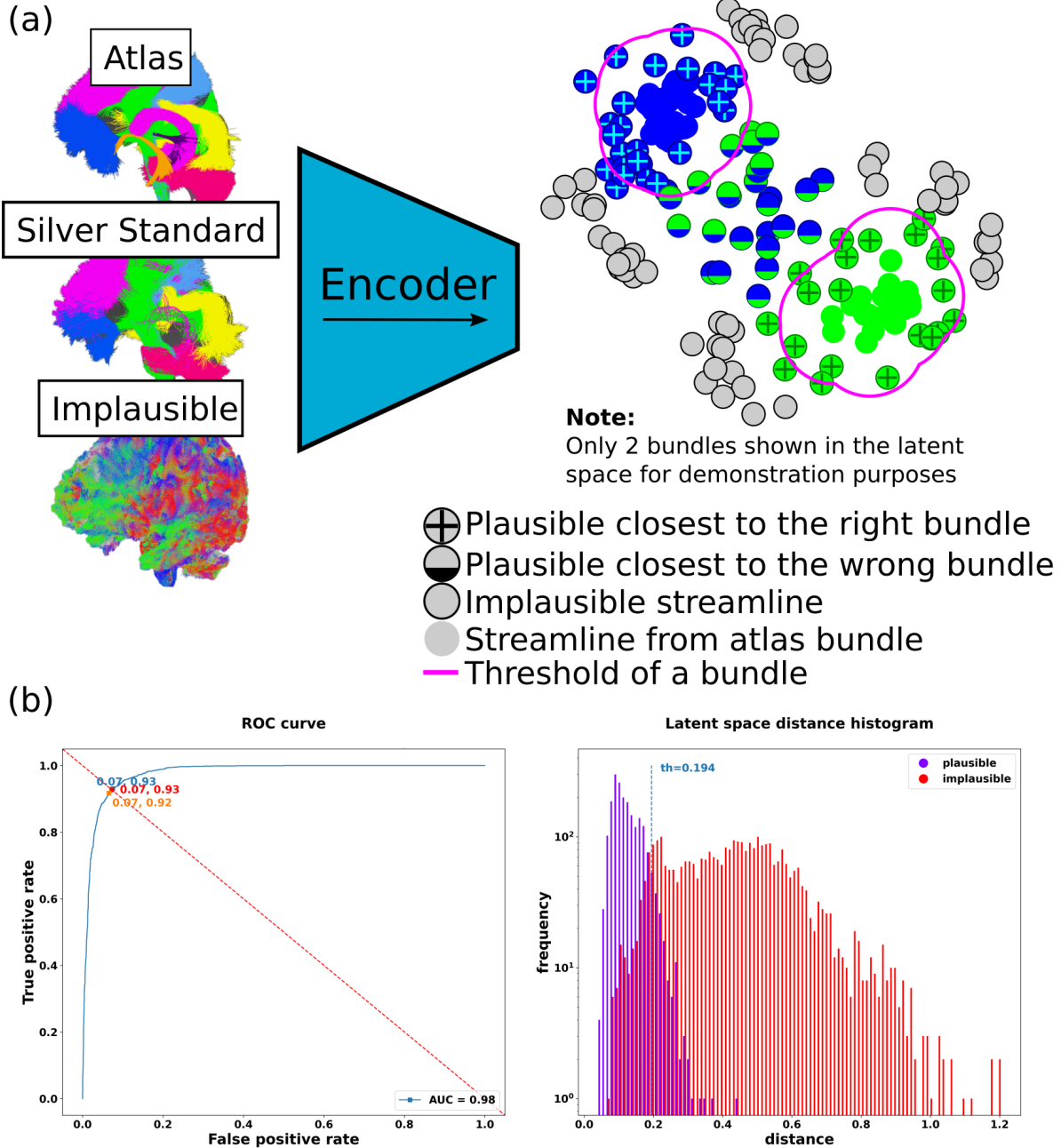


Figure 3: Threshold calibration steps where (a) atlas, silver standard, and implausible streamlines in MNI space are projected in the latent space. *Optimal* thresholds are found by assigning all silver standard and implausible streamlines to the class of the closest atlas streamline and by balancing true positives and false positives for each bundle. (b) For each bundle in the atlas, the inverse diagonal of the ROC curve, built from the right silver standard streamlines assigned to the current atlas bundle (interpreted as positive streamlines) and the wrong silver standard combined with the implausible streamlines assigned to the current atlas bundle (interpreted as negative streamlines), is used to find the optimal threshold. **Left:** *optimal* threshold for 1 bundle found at the intersection of the ROC curve with the inverse diagonal and **Right:** histogram of one bundle with the x-axis giving the distance to the closest streamline in the atlas to each streamline in the silver standard (plausible) and implausible streamlines. The *optimal* distance threshold found with the ROC curve analysis is indicated.

new streamlines does not affect the bundle volume significantly, the bundle is saturated, i.e., it is “well filled”. We

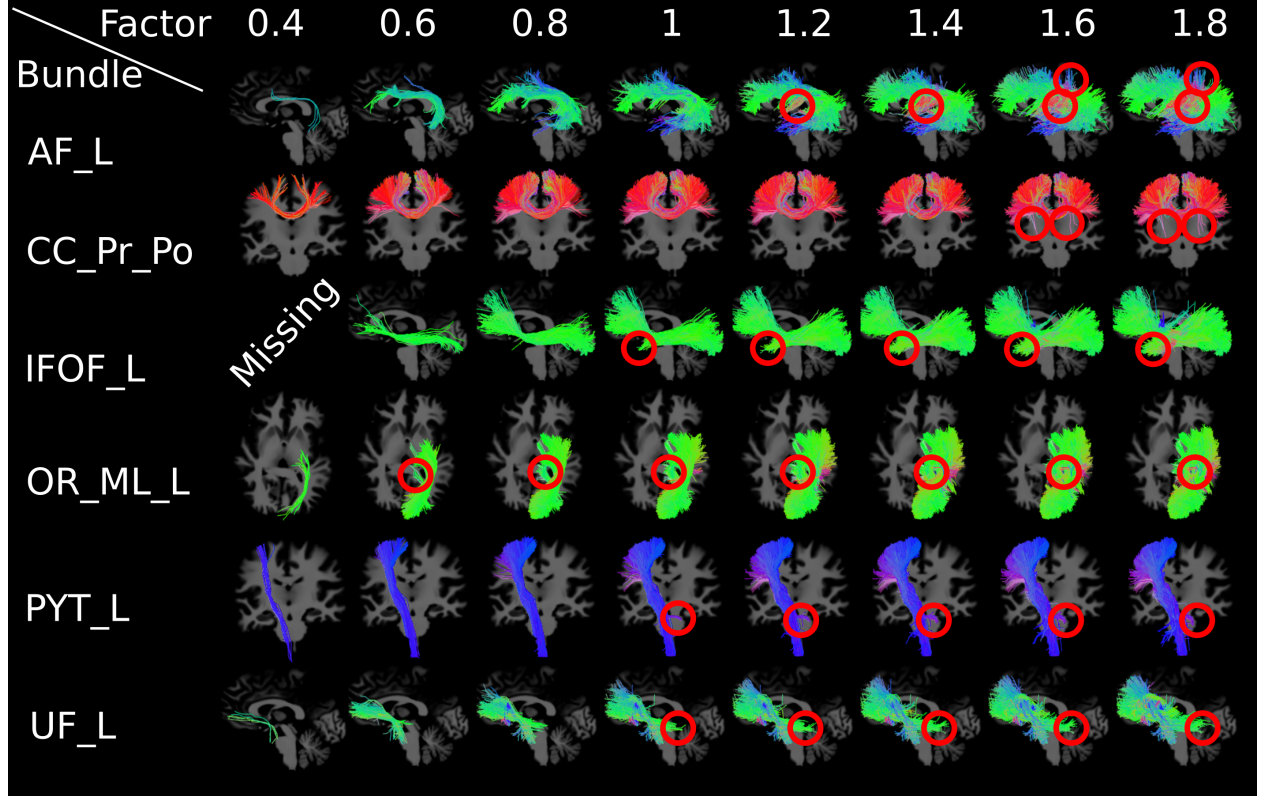


Figure 4: Effect of various factors based on automated thresholds found with ROC curves analysis where a factor of 1 represents the original thresholds. Factors below 1 mean that original thresholds were reduced, while factors above 1 mean that original thresholds were increased. Red circles indicate false positive streamlines according to atlas ideal bundles presented in Fig. 2. *Missing* means that the method did not extract any streamline for a particular bundle.

analyzed saturation curves [62, 20] of bundle volumes from the FIESTA-gen process compared to the streamline count over 5 bundles based on a whole-brain tractogram of 1 million streamlines. To generate such saturation curves, we produced bundles with 25,000 streamlines **post FIESTA-gen filtering**. After, we logarithmically randomly sampled with replacement 50 subsampled bundles from each bundle. The volume was then computed for each sub-bundle. Fig. 5 presents the saturation curves for those 5 bundles – namely the AF_L, the UF_L, the CC_Pr_Po, the IFOF_L, and the PYT_L. We see that, after 5000 generated streamlines, each bundle volume starts to saturate and after 15,000, no real volume gain is obtained from the generative process. Therefore, we fixed the number of latent-sampled vectors to 25,000 prior to decoding in our experiments, where about half the generated bundles had a final count of more than 5000 streamlines. Finally, bundles with less final streamlines were generally caused, not by a wrongful generative process, but by imperfect WM masks or bundle atlas alignments with the underlying standard space anatomy.

2.5 Reliability evaluation metrics

FIESTA's test-retest reliability was assessed using the *MyeloInferno* dataset according to five overlap metrics – namely (i) the voxel-wise dice coefficient, (ii) the weighted voxel-wise dice coefficient, (iii) the voxel-wise bundle adjacency, (iv) the streamline-wise bundle adjacency, and (v) the streamline density correlation [13, 63, 64]. The dice and the weighted dice coefficients are overlap measures between 2 bundles varying from 0 to 1 where 1 means a perfect overlap. The weighted dice score is weighted by the number of streamlines in each voxel. Bundle adjacency measures are distance metrics, similar to the Hausdorff distance [65], which yield an average distance between 2 bundles. Metrics are reported in mm and, while there is no cap for those metrics, a value of 0 mm means that there is no distance between 2 bundles. Finally, the streamline density correlation yields a simple Pearson correlation between 2 bundle density maps going from 0 to 1 with 1 meaning that those 2 bundles are perfectly correlated. Intra-subject tractography variability was assessed pairwise, i.e., for a total of J acquisitions per subject, metrics were computed between images $[1 \rightarrow 2, 1 \rightarrow 3, 1 \rightarrow 4, \dots, J-1 \rightarrow J]$ equaling to a total of $J(J-1)/2$ comparisons per bundle. Also, to gauge FIESTA's reproducibility we computed the intraclass correlation coefficient (ICC) over volume, and average bundle

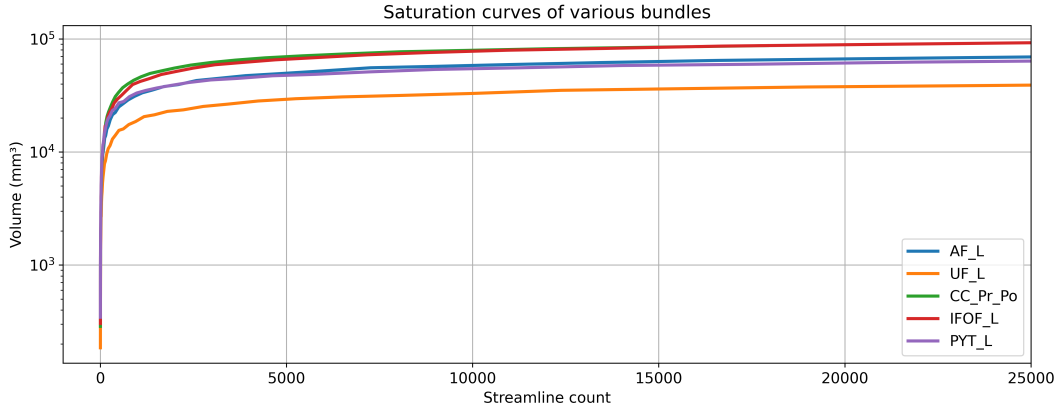


Figure 5: Saturation curves of various bundles generated by FIESTA-gen showing that between 5000 and 15,000 is a reasonable amount of generated streamlines to cover the entirety of the bundle. After 15,000 streamlines, the volume of each bundle does not increase significantly.

lengths. Based on Koo and Li (2016) [66], ICC estimates and their 95% confidence intervals were computed based on a two-way mixed-effects, consistency, multiple raters/measurements model (ICC (3,k)). Implementation was done using the Pingouin statistical Python package (v0.5.1) [67].

2.6 Hyperparameters

The final fixed hyperparameters used for FIESTA were a generative sampling of 25,000 new streamlines based on 10,000 seed points from an atlas/subject bundle ratio of [0.5 : 0.5] followed by the FIESTA-gen filtering process. It should also be noted that, for bundles where FIESTA-seg was not able to give 50% of the 10,000 required seeds, atlas bundle streamlines were used to compensate.

2.7 Methods' comparison

To have a broad range of comparisons, we benchmarked our method against 5 state-of-the-art bundling methods — namely *RecoBundles* (RB) [19], *RecoBundlesX* (RBx) [20], *TractSeg* [10, 21, 22, 23], *XTRACT* [24], and *White Matter Analysis* (WMA) [25, 26, 27]. We also compared FIESTA-seg against FIESTA (FIESTA-seg + FIESTA-gen) to see the effect of generative sampling on bundles' reliability. While *RecoBundles*, *RecoBundlesX*, WMA, FIESTA-seg, and FIESTA used the whole-brain tractogram from *TractoFlow*, we used the default tracking algorithm for *TractSeg* and *XTRACT*. Also, as *XTRACT* software yields bundle density maps, the evaluation was done on thresholded maps with a value of 0.5% of the highest bundle value. WMA whole-brain tractogram's had to be downsampled to 500,000 streamlines due to algorithmic computational limitations. In comparison, *RecoBundles*, *RecoBundlesX*, FIESTA-seg, and FIESTA whole-brain tractograms were not downsampled and used the ~4M streamlines yielded by *TractoFlow*.

Since the 5 bundling methods against which FIESTA is compared do not have the same bundle names and/or definitions, as a matter of fairness, only the similar bundles from all methods were compared together. Therefore, 27 similar bundles are kept for the analysis since some bundles in *TractSeg*, WMA, and *XTRACT* had completely different definitions than that of FIESTA. All compared bundles from each method can be found in Supplemental section A.4. It should be noted that WMA misses the SCP bundle, while *XTRACT* only shared 17 similar bundles compared to the other methods. Thus, the global average results were computed on those 17 bundles, whilst individual results were computed on the 27 bundles shared amongst the method.

3 Results

3.1 Qualitative Analysis

To gain insight into the different methods, we conducted a qualitative analysis on a random subject from the *MyeloInferno* dataset. Fig. 6 lays out the same bundles across each bundling method for a given subject. First, it is qualitatively seen that FIESTA's results (which contains generated streamlines), seems to have the best hemispheric homogeneity. This is

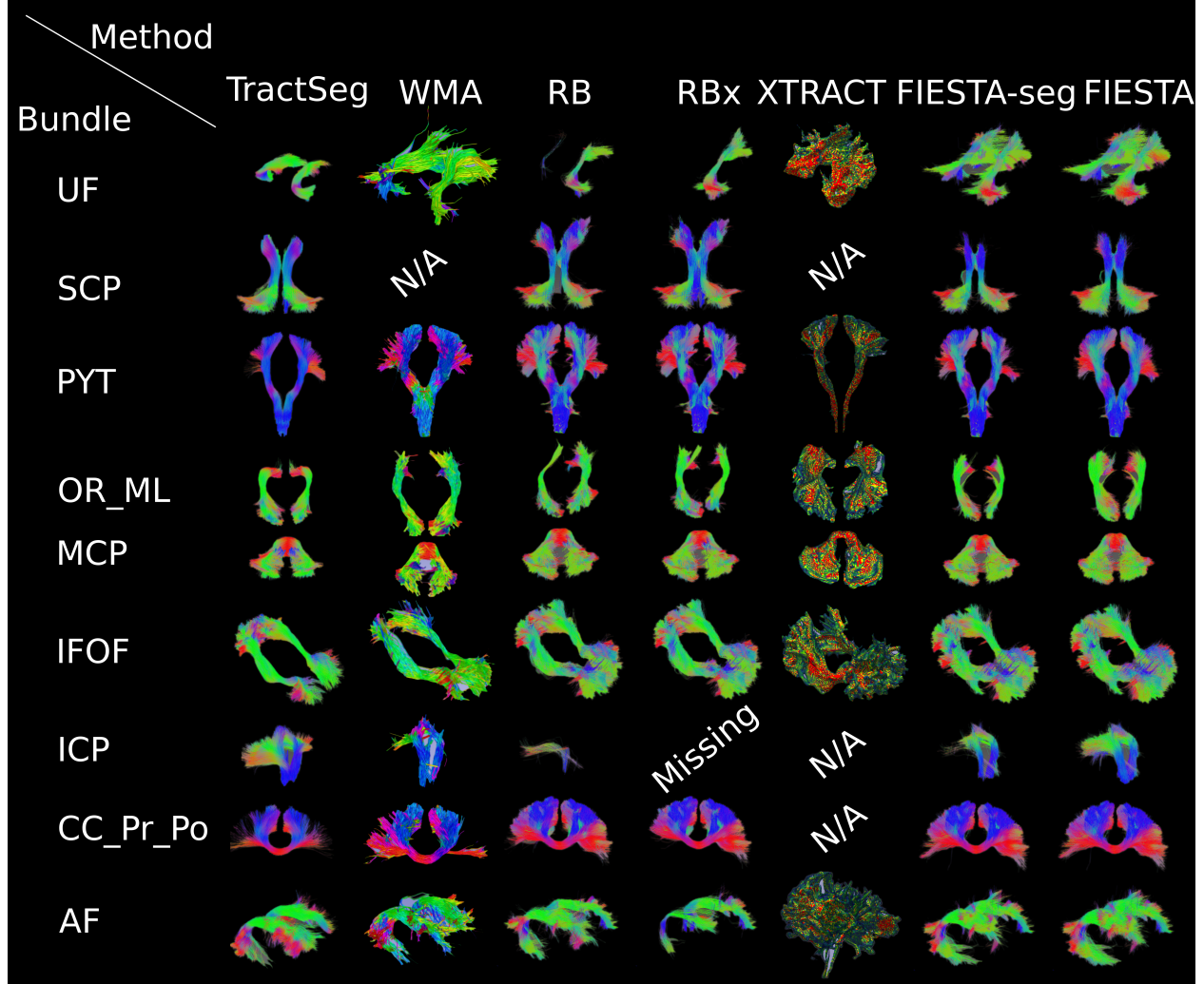


Figure 6: Qualitative results for a subset of bundles from the different benchmarked methods from one *MyeloInferno* subject. *N/A* means that the bundle was not included in the method, while *Missing* means that the method failed to extract that bundle. Lateral bundles (in both hemispheres) are shown jointly: UF, SCP, PYT, OR_ML, IFOF, ICP, and AF. *XTRACT* bundles show density maps (thresholded at 0.5%).

particularly true for the PYT and the CC_Pr_Po bundles. *TractSeg* misses some WM streamlines on the left PYT and the CC_Pr_Po bundles. Otherwise, *TractSeg* and WMA seem to output cleaned bundles with few spurious streamlines. The major drawback of WMA comes from its inability to process the original tractograms due to memory issues (~ 4 M streamlines in the *MyeloInferno* dataset for each whole-brain tractogram). *RecoBundles* and *RecoBundlesX* seem to be the least effective methods. For *RecoBundlesX*, the left UF is almost empty, while the left ICP is missing. The same goes for *RecoBundlesX* with a completely missing ICP (left and right) and a missing left UF. Also, comparing their SCP to that from the atlas (c.f. Fig. 2), it is seen that several of those streamlines belong to the medulla, which were not included in the atlas bundles. *XTRACT* retrieves almost all streamlines for each bundle. Unfortunately, *XTRACT* has a high sensitivity but a low specificity for some bundles such as the AF, the UF, and the OR. Finally, FIESTA-seg clusters correctly all bundles, but with an inhomogeneous fanning for the PYT, while FIESTA does not have any obvious problems.

3.2 Reliability Analysis

Table 1 presents the results of the average similarity metrics for each method benchmarked over 17 similar bundles, all shared among the different methods. Quantitative average results showed that FIESTA yielded the best dice, voxel-wise dice, voxel-wise bundle adjacency, and streamline density correlation with 0.74 ± 0.08 , 0.96 ± 0.04 , 0.43 ± 0.21 mm, and 0.85 ± 0.13 respectively, whereas FIESTA-seg obtained the best streamline-wise bundle adjacency with a value of

5.02 ± 0.54 mm. The voxel-wise bundle adjacency shows that, on average, two binary masks of the same bundle from the same subject are ~ 0.5 mm apart using FIESTA. For each metric where FIESTA did not come up first, it was in the margin of error of the first one. *TractSeg* yielded the best ICC length and ICC volume with values of 0.79 ± 0.05 and 0.82 ± 0.06 , respectively, whereas FIESTA yielded 0.79 ± 0.05 and 0.81 ± 0.07 , respectively. FIESTA-seg yielded the best streamline-wise bundle adjacency (5.02 ± 0.54 mm), whilst FIESTA yielded 5.24 ± 0.44 mm. Finally, according to Koo and Li (2016) [66], ICCs yielded by FIESTA show that the method has a good reliability.

Table 1: Average (\pm SD) similarity metric values and ICC for the 17 studied bundles, shared across different state-of-the-art methods. Up and down arrows mean that higher and lower are better respectively for the studied metric. V. and S. stand for Voxels and Streamlines. L. stands for Length. B. A. stands for Bundle Adjacency. It should be noted that the bundle adjacency streamlines and the ICC length was not computed for *XTRACT* because the software outputs streamline density volume maps instead of WM streamlines for each bundle.

17 Bundles	<i>TractSeg</i>	RB	RBx	WMA	<i>XTRACT</i>	FIESTA-seg	FIESTA
Dice V. (\uparrow)	0.65 ± 0.10	0.56 ± 0.22	0.58 ± 0.23	0.56 ± 0.11	0.64 ± 0.15	0.71 ± 0.09	0.74 ± 0.08
W-Dice V. (\uparrow)	0.85 ± 0.09	0.78 ± 0.29	0.79 ± 0.29	0.78 ± 0.14	0.84 ± 0.14	0.94 ± 0.06	0.96 ± 0.04
B. A. V. (mm) (\downarrow)	0.70 ± 0.45	1.65 ± 2.03	1.46 ± 2.01	0.88 ± 0.39	0.89 ± 0.63	0.51 ± 0.27	0.43 ± 0.21
B. A. S. (mm) (\downarrow)	5.37 ± 0.92	7.82 ± 3.01	6.94 ± 2.76	6.07 ± 0.65	N/A	5.02 ± 0.54	5.24 ± 0.44
Density Corr. (\uparrow)	0.64 ± 0.18	0.60 ± 0.30	0.64 ± 0.30	0.58 ± 0.22	0.63 ± 0.21	0.81 ± 0.15	0.85 ± 0.13
ICC L. (\uparrow)	0.79 ± 0.05	0.55 ± 0.28	0.67 ± 0.19	0.78 ± 0.08	N/A	0.78 ± 0.06	0.79 ± 0.06
ICC V. (\uparrow)	0.82 ± 0.06	0.24 ± 1.54	0.70 ± 0.13	0.73 ± 0.15	0.67 ± 0.17	0.80 ± 0.09	0.81 ± 0.07

Fig. 7 presents per-bundle similarity metric results of the 27 benchmarked bundles. It should be noted that *XTRACT* only presents 17 bundles and WMA 25 (the SCP is not present). Except for the streamline-Wise bundle adjacency, where FIESTA-seg is clearly superior, FIESTA is globally more reliable with better overall scores. The improvement is particularly important over small and hard-to-track bundles such as the ICP, the SCP, the OR_ML or the UF. More specifically, the streamline density correlation, the dice score and the weighted dice score (Fig. 7a, 7b, and 7c), show that FIESTA yields higher within-bundle similarity. Fig. 7a shows that the streamline density between different acquisitions is systematically more correlated when using FIESTA than with the other methods. The voxel-wise bundle adjacency of FIESTA shows that the average distance between 2 bundle masks of the same subject is ~ 0.5 mm. Knowing that the voxel size of the *MyeloInferno* dataset is 2 mm isotropic, this underlines how reproducible FIESTA is. Finally, Fig. 7e shows that, depending on the studied bundle, the *TractSeg* streamline-wise bundle adjacency is close to FIESTA and FIESTA-seg, with many bundles surpassing the proposed method, whilst never surpassing FIESTA-seg.

According to Fig. 7e, FIESTA-seg shows the closest scores to FIESTA with *RecoBundles*, *RecoBundlesX*, and WMA's being less reproducible. In comparison, *RecoBundles*, *RecoBundlesX*, FIESTA-seg, and FIESTA had about 4,000,000 input streamlines. This might explain why WMA seems to perform poorly, as we had to down sample the input whole-brain tractogram due to the computational cost of the method.

According to the charts in Fig. 7b and Fig. 7c, FIESTA is less effective for the ICP bundle. To better understand this behavior, we further investigated the case. Fig. 8 shows the left ICP produced by FIESTA on the subject with the poorest similarity metrics. We see that the variability for this particular bundle is explained by the positioning of the MRI field of view, which seems to cut at various points in the brainstem. Therefore, the starting zones of the ICP are variable. Despite this bundle variability, Fig. 8 shows that FIESTA is robust to such starting zone variations.

To complement the previous results, Fig. 9 shows the reliability scores with respect to bundle-wise metrics – namely volume and average length. Following Koo and Li (2016) [66] guidelines, an ICC between 0.75 and 0.9 and above 0.9 are respectively indicative of good and excellent reliability. Fig. 9a presents the ICC of the bundle average length, which provides insight into the reliability of each method to obtain the average bundle length values. FIESTA outperforms *RecoBundles* and *RecoBundlesX* in most bundles. WMA and *TractSeg* are more competitive than anticipated. Careful analysis reveals that although average overlap metrics for those methods are much worse than FIESTA, they yield streamlines with consistent lengths across various time points. It can be seen in Fig. 7e, that *TractSeg* seems to produce a high streamline-wise bundle adjacency. The per-bundle volume measurement results in Fig. 9b shows a similar trend with *TractSeg*, FIESTA-seg, and FIESTA having comparable results, and *TractSeg* and FIESTA-seg outperforming FIESTA for some bundles. This might be explained by the fact that *TractSeg* uses probabilistic bundle specific tracking instead of whole-brain tracking. But although the *TractSeg* bundle-wise volume is stable through different time-points, its test-retest similarity metrics are much worse than FIESTA. Finally, even if some methods seem to yield higher ICC values than FIESTA, most FIESTA's ICC were higher than 0.75, thus producing good reliability measurement (c.f. Table 1).

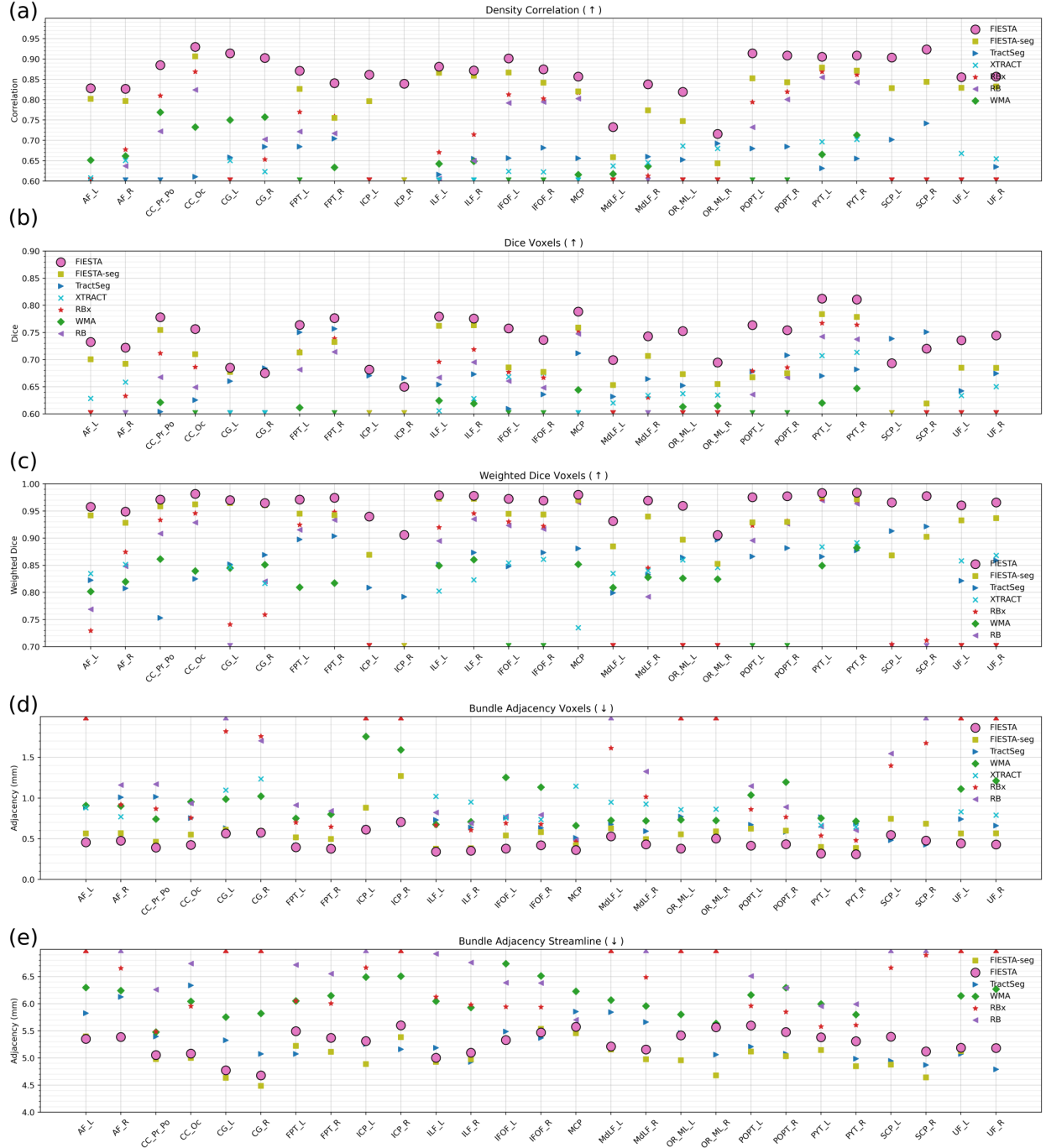


Figure 7: Average per-bundle overlap metrics. Each metric was computed over 5 acquisitions from 18 subjects registered to the MNI152 template with per subject pairwise comparison yielding 10 comparisons per subject. For visualization purposes, only the 27 most similar bundles across methods are shown. It should be noted that the SCP was not present in the bundles from WMA. *XTRACT* also misses all CC bundles, the FPT, the ICP, the POPT, and the SCP. (a) Streamline Density Correlation, (b) Voxel-Wise Dice Score Coefficient, (c) Weighted Voxel-Wise Dice Score Coefficient, (d) Voxel-Wise Bundle Adjacency, and (e) Streamline-Wise Bundle Adjacency. The streamline-wise bundle adjacency was not computed for *XTRACT* because the software outputs streamline density volume maps instead of WM streamlines for each bundle. The legend of each chart presents, from top to bottom, the method with the best average metric value according to Table 1. Outlier values are clipped to the bottom or top of each chart and are displayed as small triangles.

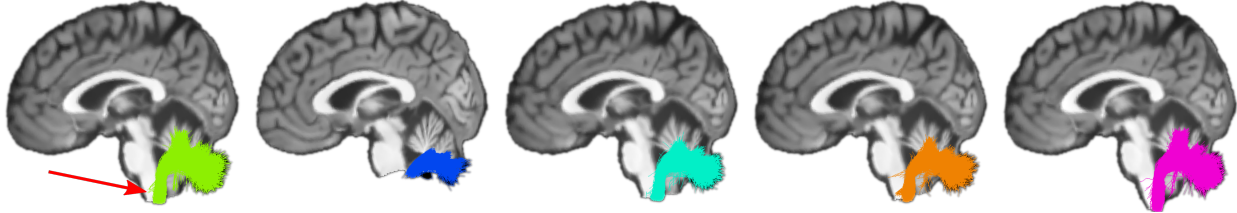


Figure 8: Visualization of FIESTA’s ICP across 5 acquisitions of the subject with the largest variability in scores. Each color stands for a different acquisition. The variability is mostly explained by the MRI field of view, and not by FIESTA’s natural variability. In that case, the ICP starts at various points of the medulla (or the pons for the second image) because the original image is cut at various points in the brainstem. Red arrow points to the medulla on the left most image.

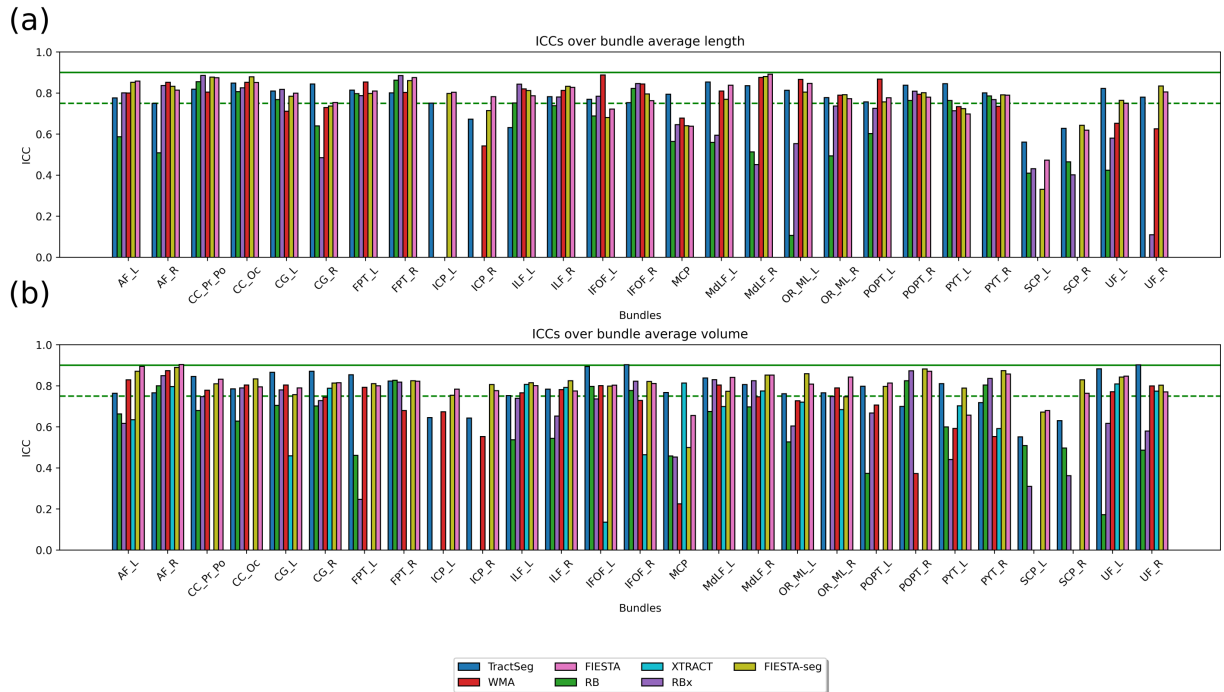


Figure 9: Bundle ICCs from the on the 27 benchmarked bundles, where (a) is the ICC based on bundle average length and (b) is the ICC based on the per-bundle voxel volume. It should be noted that the ICC length was not computed for *XTRACT* because the software outputs streamline density volume maps instead of WM streamlines for each bundle. Green dotted lines indicate good reliability (0.75) and Green hard lines indicate excellent reliability (0.9).

4 Discussion

Automatic bundling is an essential processing step in tractography to isolate specific white matter pathways. In this study, we have presented a novel semi-supervised autoencoder-based automatic bundling method called FIESTA (*FIber gEneration and bundle Segmentation in Tractography using Autoencoders*). We compared FIESTA’s reliability to state-of-the-art automatic bundling methods – namely *RecoBundles* (RB) [19], *RecoBundlesX* (RBx) [20], *TractSeg* [10, 21, 22, 23], *XTRACT* [24], and *White Matter Analysis* (WMA) [25, 26, 27]. We found that methods such as *RecoBundles* and *RecoBundlesX* are prone to large intra and inter-subject variability. Bundle definitions from *TractSeg* are fixed, requiring a complete retraining of the system for a different set of bundles. From a practical point of view, it would be hardly doable to change a specific bundle definition overnight, as one would need to create a completely new training set to train all three U-Nets. WMA is too computationally expensive. We had to downsample input tractograms to 500,000 streamlines. *XTRACT* ROIs seem to yield bundles with a low specificity and are hardly editable because they are defined by 5 anatomical experts, which would be time-consuming to change. Finally, we found that FIESTA is robust to these problems present in current state-of-the-art bundling methods.

As mentioned, the main goal of this work is to assess the reliability of FIESTA alongside state-of-the-art automatic bundling methods. As per many segmentation algorithms in biomedical image analysis, we claim that reliability analysis are as important as standard comparisons to some ground truth (or silver standard). It gives a better insight of the robustness of the method, even if the comparison to the ground truth is poor. Therefore, both validation methods are as important, but the reliability is often rarely reported. Results presented in Table 1 show that FIESTA yields reliable bundles suggested by different similarity metrics (Dice, weighted-Dice, voxel-wise bundle adjacency, streamline-wise bundle adjacency and streamline density correlation) in a test-retest manner over different dMRI time points. Quantitative average results showed that FIESTA yielded the best Dice, voxel-Wise bundle adjacency, and streamline density correlation or is in the margin of error of the best values (streamline-wise bundle adjacency, ICC length, and ICC volume). The voxel-wise bundle adjacency shows that, on average, two binary masks of the same bundle from the same subject are ~ 0.5 mm apart using FIESTA. This value is minimal considering that the acquisition resolution of the dataset used is 2 mm isotropic. Also, variability induced by registration, necessary for similarity metric computations, did not overly affect the voxel-wise bundle adjacency average distance. Higher density correlation obtained by FIESTA might be explained, in part, by the use of generative sampling. Interestingly, a closer analysis of the source of variability in FIESTA reveals that it is mainly due to the MRI field of view positioning (c.f. Fig. 8).

ICC results are not as consistent as it is the case for similarity metrics. It is seen that bundles from *TractSeg* are more reliable for volume and average length. This is probably due to the fact that *TractSeg* uses probabilistic bundle-specific tracking and not whole-brain tracking for bundle extraction later on. Thus, it probably yields more consistent metrics at various time points depending on the studied bundle. Following those results, we claim that the interpretation of any ICCs, especially in biomedical image analysis, needs to be interpreted cautiously. Indeed, a bad algorithm could, for example, produce, by chance, bundles with the same volume without being in the same anatomical region. Thus, it would yield high ICCs, with low overlap values. Therefore, the interpretability of an ICC must always be paired, within the context of a tractography analysis, with similarity metrics and a good qualitative analysis.

FIESTA is not a method without flaws. First, we see that the use of generative sampling does worsen the streamline-wise bundle adjacency. We hypothesized that such behavior might be due to an increase amount of broken streamlines yielded by the generative sampling. Also, using the atlas bundles as seeds for the latent space might produce more anatomical generic bundles instead of subject specific bundles. Such behavior is currently under investigation and generative sampling filter parameter might need further adjustment. Second, the threshold calibration, even though it can be done quickly compared to other state-of-the-art methods, is probably the most time-consuming process. A solution would be to get rid of the threshold method by including a new *bundle* in the atlas with all whole-brain implausible WM streamlines. Therefore, streamlines closer to the implausible *bundle* would be classified as implausible. New bundle definitions could easily be implemented, as only an ideal bundle in a standard space would be needed for the change to be effective, without the need to find/calibrate any threshold. As WMA uses this method for implausible streamlines, it might be pertinent to test. Unfortunately, this method also has its limitations, as defining implausible streamlines is an open and hard problem to solve. Also, even if we presented a solution to find the *optimal* threshold in section 2.3.1, the most easy way to find the desired threshold, whilst being the least sophisticated method, is just to test a few thresholds manually, starting completely randomly and slowly converging around the desired final values. Finally, the generative sampling method takes a long time for certain bundles. It would be interesting to include per-bundle generative sampling parameters to optimize the pipeline [31].

This work mainly focuses on the bundling of long-range white matter streamlines, that connect distant cortical areas of the brain. We did not assess the behavior of FIESTA on short association fibers (U-Fibers) [68] that connect adjacent cortical regions. Future works will include the evaluation of FIESTA on such fibers.

5 Conclusion

We presented a new tractography bundling pipeline named FIESTA (*FIber gEneration and bundle Segmentation in Tractography using Autoencoders*) that leverages the power of unsupervised and self-supervised learning and that is intended as a solution to the limitations of current state-of-the-art bundling pipelines. We showed that FIESTA lets users easily and rapidly edit its bundle definitions, and is highly reliable in test-retest. FIESTA is more reliable than other state-of-the-art methods such as *TractSeg*, *RecoBundles*, *RecoBundlesX*, *XTRACT*, and WMA. We believe FIESTA reaches an optimal compromise between computational burden, ease-of-use, and reconstruction quality and reliability. Thus, FIESTA might be a promising avenue as an easy and reliable way for bundling in tractography, especially so for hard-to-track bundles.

Data/code availability

All data used to develop and test FIESTA were acquired from different public (TractoInferno, HCP, PAWM atlas) and private datasets (MyeloInferno). Data from the MyeloInferno dataset cannot be made public to respect ethics protocol from the institution. URL links for public datasets are:

1. TractoInferno: <https://openneuro.org/datasets/ds003900>
2. HCP: <http://www.humanconnectomeproject.org/>
3. PAWM atlas: <https://doi.org/10.5281/zenodo.5165374>

The source code will be made available to the community upon the acceptance of the article under the <https://github.com/scil-vital> GitHub organization.

Ethics statement

Written informed consent was obtained from participants and were recruited following the ethics protocol of the Centre de Recherche du Centre Hospitalier Universitaire de Sherbrooke (for the MyeloInferno dataset).

Acknowledgments

This research was conducted in the context of the Acuity-QC group funded by the Fond d'Accélération des Collaborations en Santé (FACS) and Consortium Québécois sur la Découverte du Médicament (CQDM). It was enabled, in part, by support provided by Calcul Québec (www.calculquebec.ca) and Compute Canada (www.computecanada.ca).

Data were provided, in part, by the Human Connectome Project, WU-Minn Consortium (Principal Investigators: David Van Essen and Kamil Ugurbil; 1U54MH091657) funded by the 16 NIH Institutes and Centers that support the NIH Blueprint for Neuroscience Research; and by the McDonnell Center for Systems Neuroscience at Washington University.

Data were provided, in part, by the OpenNeuro database (<https://openneuro.org/datasets/ds003900>). Its accession number is ds003900.

Conflicts of Interest

Maxime Descoteaux and Pierre-Marc Jodoin report membership and employment with Imeka Solutions inc. Patent #17/337,413 is pending to Imeka Solutions inc. with inventors Jon Haitz Legarreta, Maxime Descoteaux and Pierre-Marc Jodoin.

References

- [1] M. Descoteaux, R. Deriche, T. R. Knosche, and A. Anwander, “Deterministic and Probabilistic Tractography Based on Complex Fibre Orientation Distributions,” *IEEE Transactions on Medical Imaging*, vol. 28, pp. 269–286, Feb. 2009. Conference Name: IEEE Transactions on Medical Imaging.
- [2] M. Descoteaux, E. Angelino, S. Fitzgibbons, and R. Deriche, “Regularized, fast, and robust analytical Q-ball imaging,” *Magnetic Resonance in Medicine*, vol. 58, no. 3, pp. 497–510, 2007. _eprint: <https://onlinelibrary.wiley.com/doi/pdf/10.1002/mrm.21277>.
- [3] J.-D. Tournier, F. Calamante, and A. Connelly, “Robust determination of the fibre orientation distribution in diffusion MRI: Non-negativity constrained super-resolved spherical deconvolution,” *NeuroImage*, vol. 35, pp. 1459–1472, May 2007.
- [4] B. Kreher, I. Mader, and V. Kiselev, “Gibbs tracking: A novel approach for the reconstruction of neuronal pathways,” *Magnetic Resonance in Medicine*, vol. 60, no. 4, pp. 953–963, 2008. _eprint: <https://onlinelibrary.wiley.com/doi/pdf/10.1002/mrm.21749>.
- [5] J.-F. Mangin, P. Fillard, Y. Cointepas, D. Le Bihan, V. Frouin, and C. Poupon, “Toward global tractography,” *NeuroImage*, vol. 80, pp. 290–296, Oct. 2013.
- [6] D. Christiaens, M. Reisert, T. Dhollander, S. Sunaert, P. Suetens, and F. Maes, “Global tractography of multi-shell diffusion-weighted imaging data using a multi-tissue model,” *NeuroImage*, vol. 123, pp. 89–101, Dec. 2015.
- [7] J.-D. Tournier, S. Mori, and A. Leemans, “Diffusion tensor imaging and beyond,” *Magnetic Resonance in Medicine*, vol. 65, no. 6, pp. 1532–1556, 2011. _eprint: <https://onlinelibrary.wiley.com/doi/pdf/10.1002/mrm.22924>.
- [8] J.-D. Tournier, F. Calamante, and A. Connelly, “MRtrix: Diffusion tractography in crossing fiber regions,” *International Journal of Imaging Systems and Technology*, vol. 22, no. 1, pp. 53–66, 2012. _eprint: <https://onlinelibrary.wiley.com/doi/pdf/10.1002/ima.22005>.
- [9] G. Girard, K. Whittingstall, R. Deriche, and M. Descoteaux, “Towards quantitative connectivity analysis: reducing tractography biases,” *NeuroImage*, vol. 98, pp. 266–278, Sept. 2014.
- [10] J. Wasserthal, P. F. Neher, and K. H. Maier-Hein, “Tract orientation mapping for bundle-specific tractography,” Tech. Rep. arXiv:1806.05580, arXiv, June 2018. arXiv:1806.05580 [cs] type: article.
- [11] F. Rheault, E. St-Onge, J. Sidhu, K. Maier-Hein, N. Tzourio-Mazoyer, L. Petit, and M. Descoteaux, “Bundle-specific tractography with incorporated anatomical and orientational priors,” *NeuroImage*, vol. 186, pp. 382–398, Feb. 2019.
- [12] E. St-Onge, A. Daducci, G. Girard, and M. Descoteaux, “Surface-enhanced tractography (SET),” *NeuroImage*, vol. 169, pp. 524–539, Apr. 2018.
- [13] F. Rheault, A. De Benedictis, A. Daducci, C. Maffei, C. M. W. Tax, D. Romascano, E. Caverzasi, F. C. Morency, F. Corriveau, F. Pestilli, G. Girard, G. Theaud, I. Zemmoura, J. Hau, K. Glavin, K. M. Jordan, K. Pomiecko, M. Chamberland, M. Barakovic, N. Goyette, P. Poulin, Q. Chenot, S. S. Panesar, S. Sarubbo, L. Petit, and M. Descoteaux, “Tractostorm: The what, why, and how of tractography dissection reproducibility,” *Human Brain Mapping*, vol. 41, no. 7, pp. 1859–1874, 2020. _eprint: <https://onlinelibrary.wiley.com/doi/pdf/10.1002/hbm.24917>.
- [14] F. Rheault, K. G. Schilling, A. Valcourt-Caron, A. Théberge, C. Poirier, G. Grenier, G. I. Guberman, J. Begnoche, J. H. Legarreta, L. Y. Cai, M. Roy, M. Edde, M. P. Caceres, M. Ocampo-Pineda, N. Al-Sharif, P. Karan, P. Bontempi, S. Obaid, S. Bosticardo, S. Schiavi, V. Sairanen, A. Daducci, L. E. Cutting, L. Petit, M. Descoteaux, and B. A. Landman, “Tractostorm 2: Optimizing tractography dissection reproducibility with segmentation protocol dissemination,” *Human Brain Mapping*, vol. 43, no. 7, pp. 2134–2147, 2022. _eprint: <https://onlinelibrary.wiley.com/doi/pdf/10.1002/hbm.25777>.
- [15] E. Garyfallidis, M. Brett, M. M. Correia, G. B. Williams, and I. Nimmo-Smith, “QuickBundles, a Method for Tractography Simplification,” *Frontiers in Neuroscience*, vol. 6, p. 175, Dec. 2012.
- [16] E. Garyfallidis, M.-A. Côté, F. Rheault, and M. Descoteaux, “QuickBundlesX: Sequential clustering of millions of streamlines in multiple levels of detail at record execution time,” in *ISMRM 2016*, Nov. 2015.
- [17] Y. Chen, C. Zhang, Y. Song, N. Makris, Y. Rathi, W. Cai, F. Zhang, and L. J. O’Donnell, “Deep Fiber Clustering: Anatomically Informed Unsupervised Deep Learning for Fast and Effective White Matter Parcellation,” *arXiv:2107.04938 [cs]*, July 2021. arXiv: 2107.04938.
- [18] Y. Chen, C. Zhang, T. Xue, Y. Song, N. Makris, Y. Rathi, W. Cai, F. Zhang, and L. J. O’Donnell, “DFC: Anatomically Informed Fiber Clustering with Self-supervised Deep Learning for Fast and Effective Tractography Parcellation,” *arXiv:2205.00627 [cs]*, May 2022. arXiv: 2205.00627.

- [19] E. Garyfallidis, M.-A. Côté, F. Rheault, J. Sidhu, J. Hau, L. Petit, D. Fortin, S. Cunanne, and M. Descoteaux, “Recognition of white matter bundles using local and global streamline-based registration and clustering,” *NeuroImage*, vol. 170, pp. 283–295, Apr. 2018.
- [20] F. Rheault, *Analyse et reconstruction de faisceaux de la matière blanche*. PhD thesis, Université de Sherbrooke, Sherbrooke, July 2020.
- [21] J. Wasserthal, P. Neher, and K. H. Maier-Hein, “TractSeg - Fast and accurate white matter tract segmentation,” *NeuroImage*, vol. 183, pp. 239–253, Dec. 2018.
- [22] J. Wasserthal, P. F. Neher, D. Hirjak, and K. H. Maier-Hein, “Combined tract segmentation and orientation mapping for bundle-specific tractography,” *Medical Image Analysis*, vol. 58, p. 101559, Dec. 2019.
- [23] J. Wasserthal, K. H. Maier-Hein, P. F. Neher, G. Northoff, K. M. Kubera, S. Fritze, A. Harneit, L. S. Geiger, H. Tost, R. C. Wolf, and D. Hirjak, “Multiparametric mapping of white matter microstructure in catatonia,” *Neuropsychopharmacology*, vol. 45, pp. 1750–1757, Sept. 2020. Number: 10 Publisher: Nature Publishing Group.
- [24] S. Warrington, K. L. Bryant, A. A. Khrapitchev, J. Sallet, M. Charquero-Ballester, G. Douaud, S. Jbabdi, R. B. Mars, and S. N. Sotropoulos, “XTRACT - Standardised protocols for automated tractography in the human and macaque brain,” *NeuroImage*, vol. 217, p. 116923, Aug. 2020.
- [25] L. O’Donnell and C.-F. Westin, “Automatic Tractography Segmentation Using a High-Dimensional White Matter Atlas,” *IEEE transactions on medical imaging*, vol. 26, pp. 1562–75, Dec. 2007.
- [26] L. J. O’Donnell, W. M. Wells, A. J. Golby, and C.-F. Westin, “Unbiased Groupwise Registration of White Matter Tractography,” in *Medical Image Computing and Computer-Assisted Intervention – MICCAI 2012* (N. Ayache, H. Delingette, P. Golland, and K. Mori, eds.), Lecture Notes in Computer Science, (Berlin, Heidelberg), pp. 123–130, Springer, 2012.
- [27] F. Zhang, Y. Wu, I. Norton, L. Rigolo, Y. Rathi, N. Makris, and L. J. O’Donnell, “An anatomically curated fiber clustering white matter atlas for consistent white matter tract parcellation across the lifespan,” *NeuroImage*, vol. 179, pp. 429–447, Oct. 2018.
- [28] F. Rheault, P. Poulin, A. V. Caron, E. St-Onge, and M. Descoteaux, “Common misconceptions, hidden biases and modern challenges of dMRI tractography,” *Journal of Neural Engineering*, vol. 17, p. 011001, Feb. 2020. Publisher: IOP Publishing.
- [29] J. H. Legarreta, L. Petit, F. Rheault, G. Theaud, C. Lemaire, M. Descoteaux, and P.-M. Jodoin, “Filtering in tractography using autoencoders (FINTA),” *Medical Image Analysis*, vol. 72, p. 102126, Aug. 2021.
- [30] J. H. Legarreta, L. Petit, P.-M. Jodoin, and M. Descoteaux, “Clustering in tractography using autoencoders (CINTA),” in *Computational Diffusion MRI (CDMRI) Medical Image Computing and Computer Assisted Intervention (MICCAI) Workshop*, (Singapore), Medical Image Computing and Computer Assisted Intervention (MICCAI) Society, 09 18-22, 2022. Accepted.
- [31] J. H. Legarreta, L. Petit, P.-M. Jodoin, and M. Descoteaux, “Generative sampling in tractography using autoencoders (GESTA),” *arXiv:2204.10891 [cs, eess, q-bio]*, Apr. 2022. arXiv: 2204.10891.
- [32] K. H. Maier-Hein, P. F. Neher, J.-C. Houde, M.-A. Côté, E. Garyfallidis, J. Zhong, M. Chamberland, F.-C. Yeh, Y.-C. Lin, Q. Ji, W. E. Reddick, J. O. Glass, D. Q. Chen, Y. Feng, C. Gao, Y. Wu, J. Ma, R. He, Q. Li, C.-F. Westin, S. Deslauriers-Gauthier, J. O. O. González, M. Paquette, S. St-Jean, G. Girard, F. Rheault, J. Sidhu, C. M. W. Tax, F. Guo, H. Y. Mesri, S. Dávid, M. Froeling, A. M. Heemskerk, A. Leemans, A. Boré, B. Pinsard, C. Bedetti, M. Desrosiers, S. Brambati, J. Doyon, A. Sarica, R. Vasta, A. Cerasa, A. Quattrone, J. Yeatman, A. R. Khan, W. Hodges, S. Alexander, D. Romascano, M. Barakovic, A. Auría, O. Esteban, A. Lemkadem, J.-P. Thiran, H. E. Cetingul, B. L. Odry, B. Mailhe, M. S. Nadar, F. Pizzagalli, G. Prasad, J. E. Villalon-Reina, J. Galvis, P. M. Thompson, F. D. S. Requejo, P. L. Laguna, L. M. Lacerda, R. Barrett, F. Dell’Acqua, M. Catani, L. Petit, E. Caruyer, A. Daducci, T. B. Dyrby, T. Holland-Letz, C. C. Hilgetag, B. Stieltjes, and M. Descoteaux, “The challenge of mapping the human connectome based on diffusion tractography,” *Nature Communications*, vol. 8, p. 1349, Dec. 2017.
- [33] L. Petit, F. Rheault, M. Descoteaux, and N. Tzourio-Mazoyer, “Half of the streamlines built in a whole human brain tractogram is anatomically uninterpretable.,” *F1000Research*, p. 1, 2021. [version 1; not peer reviewed].
- [34] D. Jörgens, M. Descoteaux, and R. Moreno, “Challenges for Tractogram Filtering,” in *Anisotropy Across Fields and Scales* (E. Özarslan, T. Schultz, E. Zhang, and A. Fuster, eds.), Mathematics and Visualization, (Cham), pp. 149–168, Springer International Publishing, 2021.
- [35] S. N. Sotropoulos and A. Zalesky, “Building connectomes using diffusion MRI: why, how and but,” *NMR in Biomedicine*, vol. 32, no. 4, p. e3752, 2019. _eprint: <https://onlinelibrary.wiley.com/doi/pdf/10.1002/nbm.3752>.

- [36] X. Wang, W. G. W., and C. Westin, “Tractography segmentation using a hierarchical dirichlet processes mixture model,” *Neuroimage*, vol. 54, no. 1, p. 290–302, 2011.
- [37] E. Visser, E. Nijhuis, J. Buitelaar, and M. Zwiers, “Partition-based mass clustering of tractography streamlines,” *Neuroimage*, vol. 54, no. 1, p. 303–312, 2011.
- [38] A. Yendiki, “Automated probabilistic reconstruction of white-matter pathways in health and disease using an atlas of the underlying anatomy,” *Frontiers in Neuroinformatics*, vol. 5, 2011.
- [39] D. Wassermann, N. Makris, Y. Rathi, M. Shenton, R. Kikinis, M. Kubicki, and C.-F. Westin, “The white matter query language: a novel approach for describing human white matter anatomy,” *Brain Structure and Function*, vol. 221, pp. 4705–4721, Dec. 2016.
- [40] G. Bertò, D. Bullock, P. Astolfi, S. Hayashi, L. Zigiotti, L. Annicchiarico, F. Corsini, A. De Benedictis, S. Sarubbo, F. Pestilli, P. Avesani, and E. Olivetti, “Classifyber, a robust streamline-based linear classifier for white matter bundle segmentation,” *NeuroImage*, vol. 224, p. 117402, Jan. 2021.
- [41] E. Garyfallidis, O. Ocegueda, D. Wassermann, and M. Descoteaux, “Robust and efficient linear registration of white-matter fascicles in the space of streamlines,” *NeuroImage*, vol. 117, pp. 124–140, Aug. 2015.
- [42] L. O’Donnell, M. Kubicki, M. Shenton, M. Dreusicke, W. Grimson, and C. Westin, “A Method for Clustering White Matter Fiber Tracts,” *AJR: American Journal of Neuroradiology*, vol. 27, pp. 1032–1036, May 2006.
- [43] L. O’Donnell and C.-F. Westin, “White Matter Tract Clustering and Correspondence in Populations,” in *Medical Image Computing and Computer-Assisted Intervention – MICCAI 2005* (D. Hutchison, T. Kanade, J. Kittler, J. M. Kleinberg, F. Mattern, J. C. Mitchell, M. Naor, O. Nierstrasz, C. Pandu Rangan, B. Steffen, M. Sudan, D. Terzopoulos, D. Tygar, M. Y. Vardi, G. Weikum, J. S. Duncan, and G. Gerig, eds.), vol. 3749, pp. 140–147, Berlin, Heidelberg: Springer Berlin Heidelberg, 2005. Series Title: Lecture Notes in Computer Science.
- [44] C. Fowlkes, S. Belongie, Fan Chung, and J. Malik, “Spectral grouping using the nyström method,” *IEEE Transactions on Pattern Analysis and Machine Intelligence*, vol. 26, pp. 214–225, Feb. 2004.
- [45] O. Ronneberger, P. Fischer, and T. Brox, “U-Net: Convolutional Networks for Biomedical Image Segmentation,” *arXiv:1505.04597 [cs]*, May 2015. arXiv: 1505.04597.
- [46] R. Hadsell, S. Chopra, and Y. LeCun, “Dimensionality Reduction by Learning an Invariant Mapping,” in *2006 IEEE Computer Society Conference on Computer Vision and Pattern Recognition - Volume 2 (CVPR’06)*, vol. 2, (New York, NY, USA), pp. 1735–1742, IEEE, 2006.
- [47] C. M. Bishop, *Pattern recognition and machine learning*. Information science and statistics, New York: Springer, 2006.
- [48] P. Poulin, G. Theaud, F. Rheault, E. St-Onge, A. Bore, E. Renaud, L. de Beaumont, S. Guay, P.-M. Jodoin, and M. Descoteaux, “TractoInferno : A large-scale, open-source, multi-site database for machine learning dMRI tractography,” *biorxiv* 2021.11.29.470422v1, pp. 1–32, 2021.
- [49] M. F. Glasser, S. N. Sotiropoulos, J. A. Wilson, T. S. Coalson, B. Fischl, J. L. Andersson, J. Xu, S. Jbabdi, M. Webster, J. R. Polimeni, D. C. Van Essen, and M. Jenkinson, “The minimal preprocessing pipelines for the Human Connectome Project,” *NeuroImage*, vol. 80, pp. 105–124, Oct. 2013.
- [50] M. F. Glasser, T. S. Coalson, E. C. Robinson, C. D. Hacker, J. Harwell, E. Yacoub, K. Ugurbil, J. Andersson, C. F. Beckmann, M. Jenkinson, S. M. Smith, and D. C. Van Essen, “A multi-modal parcellation of human cerebral cortex,” *Nature*, vol. 536, pp. 171–178, Aug. 2016.
- [51] M. Edde, G. Theaud, M. Dumont, A. Théberge, A. Valcourt-Caron, S. Magon, and M. Descoteaux, “Measures of reliability in high frequency longitudinal white matter multi-shell diffusion and inhomogeneous magnetization transfer database,” in *ISMRM 2022*, p. 3, Oct. 2021.
- [52] G. Theaud, M. Edde, M. Dumont, C. Zotti, M. Zucchelli, S. Deslauriers-Gauthier, R. Deriche, P.-M. Jodoin, and M. Descoteaux, “DORIS: A diffusion MRI-based 10 tissue class deep learning segmentation algorithm tailored to improve anatomically-constrained tractography,” *Frontiers in Neuroimaging*, vol. 1, 2022.
- [53] G. Theaud, J.-C. Houde, A. Boré, F. Rheault, F. Morency, and M. Descoteaux, “TractoFlow: A robust, efficient and reproducible diffusion MRI pipeline leveraging Nextflow & Singularity,” *NeuroImage*, vol. 218, p. 116889, Sept. 2020.
- [54] F. Rheault, “Population average atlas for RecobundlesX (1.1).” <https://doi.org/10.5281/zenodo.5165374>, 2021. [Data set].
- [55] L. Petit, K. M. Ali, F. Rheault, A. Boré, S. Cremona, F. Corsini, A. De Benedictis, M. Descoteaux, and S. Sarubbo, “The structural connectivity of the human angular gyrus as revealed by microdissection and diffusion tractography,” *Brain Structure and Function*, Aug. 2022.

- [56] G. E. Hinton and R. R. Salakhutdinov, “Reducing the Dimensionality of Data with Neural Networks,” *Science*, vol. 313, pp. 504–507, July 2006.
- [57] I. Goodfellow, Y. Bengio, and A. Courville, *Deep Learning*. The MIT Press, Nov. 2016.
- [58] V. Fonov, A. Evans, R. McKinstry, C. Almlí, and D. Collins, “Unbiased nonlinear average age-appropriate brain templates from birth to adulthood,” *NeuroImage*, vol. 47, p. S102, July 2009.
- [59] V. Fonov, A. C. Evans, K. Botteron, C. R. Almlí, R. C. McKinstry, and D. L. Collins, “Unbiased average age-appropriate atlases for pediatric studies,” *NeuroImage*, vol. 54, pp. 313–327, Jan. 2011. Num Pages: 313-327 Place: Amsterdam, United States Publisher: Elsevier Limited.
- [60] B. W. Silverman, *Density Estimation for Statistics and Data Analysis*, vol. 26 of *Monographs on Statistics and Applied Probability*. Chapman and Hall, 1986.
- [61] N. Painchaud, Y. Skandarani, T. Judge, O. Bernard, A. Lalande, and P.-M. Jodoin, “Cardiac Segmentation With Strong Anatomical Guarantees,” *IEEE Transactions on Medical Imaging*, vol. 39, pp. 3703–3713, Nov. 2020. Conference Name: IEEE Transactions on Medical Imaging.
- [62] A. Gauvin, “Assurance qualité en dissection virtuelle des faisceaux de la matière blanche par tractographie,” Master’s thesis, 2016.
- [63] M. Cousineau, P.-M. Jodoin, E. Garyfallidis, M.-A. Côté, F. C. Morency, V. Rozanski, M. Grand’Maison, B. J. Bedell, and M. Descoteaux, “A test-retest study on Parkinson’s PPMI dataset yields statistically significant white matter fascicles,” *NeuroImage: Clinical*, vol. 16, pp. 222–233, Jan. 2017.
- [64] L. R. Dice, “Measures of the Amount of Ecologic Association Between Species,” *Ecology*, vol. 26, no. 3, pp. 297–302, 1945. Publisher: Ecological Society of America.
- [65] R. T. Rockafellar and R. J.-B. Wets, *Variational Analysis*. Springer Science & Business Media, July 2009.
- [66] T. K. Koo and M. Y. Li, “A Guideline of Selecting and Reporting Intraclass Correlation Coefficients for Reliability Research,” *Journal of Chiropractic Medicine*, vol. 15, pp. 155–163, June 2016.
- [67] R. Vallat, “Pingouin: statistics in Python,” *Journal of Open Source Software*, vol. 3, p. 1026, Nov. 2018.
- [68] D. Shastin, S. Genc, G. D. Parker, K. Koller, C. M. Tax, J. Evans, K. Hamandi, W. P. Gray, D. K. Jones, and M. Chamberland, “Surface-based tracking for short association fibre tractography,” *NeuroImage*, vol. 260, p. 119423, Oct. 2022.
- [69] C. Sudlow, J. Gallacher, N. Allen, V. Beral, P. Burton, J. Danesh, P. Downey, P. Elliott, J. Green, M. Landray, B. Liu, P. Matthews, G. Ong, J. Pell, A. Silman, A. Young, T. Sprosen, T. Peakman, and R. Collins, “UK Biobank: An Open Access Resource for Identifying the Causes of a Wide Range of Complex Diseases of Middle and Old Age,” *PLOS Medicine*, vol. 12, p. e1001779, Mar. 2015. Publisher: Public Library of Science.
- [70] E. Garyfallidis, M. Brett, B. Amirbekian, A. Rokem, S. van der Walt, M. Descoteaux, and I. Nimmo-Smith, “Dipy, a library for the analysis of diffusion MRI data,” *Frontiers in Neuroinformatics*, vol. 8, Feb. 2014.
- [71] B. B. Avants, N. J. Tustison, G. Song, P. A. Cook, A. Klein, and J. C. Gee, “A reproducible evaluation of ANTs similarity metric performance in brain image registration,” *NeuroImage*, vol. 54, pp. 2033–2044, Feb. 2011.
- [72] C. Presseau, P.-M. Jodoin, J.-C. Houde, and M. Descoteaux, “A new compression format for fiber tracking datasets,” *NeuroImage*, vol. 109, pp. 73–83, Apr. 2015.

A Appendices

A.1 Bundles used for experiments

Table A.1: Original 39 bundles provided in the PAWM atlas [54]. Labels with only one number indicate that there is no lateral symmetry for this particular bundle.

Name	Abbreviation	Left	Right
Anterior Commissure	AC	1	
Arcuate Fasciculus	AF	2	3
Corpus callosum, Frontal Lobe (most anterior part)	CC_Fr_1	4	
Corpus callosum, Frontal Lobe (most posterior part)	CC_Fr_2	5	
Corpus callosum, Occipital Lobe	CC_Oc	6	
Corpus callosum, Parietal Lobe	CC_Pa	7	
Corpus callosum, Pre- / Post-Central Gyri	CC_Pr_Po	8	
Corpus callosum, Temporal Lobe	CC_Te	9	
Cingulum	CG	10	11
Frontal Aslant Tract	FAT	12	13
Fronto-Pontine Tract	FPT	14	15
Fornix	FX	16	17
Inferior cerebellar peduncle	ICP	18	19
Inferior Fronto-Occipital Fasciculus	IFOF	20	21
Inferior Longitudinal Fasciculus	ILF	22	23
Middle Cerebellar Peduncle	MCP		24
Middle Longitudinal Fasciculus	MdLF	25	26
Optic Radiation and Meyer's loop	OR_ML	27	28
Posterior Commissure	PC		29
Parieto-Occipito Pontine Tract	POPT	30	31
Pyramidal Tract	PYT	32	33
Superior Cerebellar Peduncle	SCP	34	35
Superior Longitudinal Fasciculus	SLF	36	37
Uncinate Fasciculus	UF	38	39

A.2 FIESTA-gen filtering parameters

Table A.2 presents criteria and threshold values used to ensure that the generated streamlines comply with the dMRI underlying signal and general anatomical constraints. Those were based on the ones used in GESTA [31]. All streamlines outside the length range used are removed. The winding angle is the maximum turning angle that a streamline can make before being removed. The local orientation angle to fODF (LOA-to-fODF) peak and rate values correspond to the minimum number of streamline local orientation vectors where the angle is lower than 30° with the closest fODF peak related to the total number of local orientation vectors in the streamline. If the ratio is smaller than 0.75, the streamline is removed. Finally, the WM coverage rate is the percentage of streamline vertices mapping to a WM voxel.

Table A.2: FIESTA-gen filtering parameters used after the rejection sampling

Filter	Value
Length range (mm)	20-220
Winding ($^\circ$)	<360
LOA-to-fODF peak ($^\circ$) and rate	$<30/0.75$
WM coverage rate	>0.95

A.3 FIESTA-gen Ratio

Using 10,000 streamlines as an empirically determined seed number for the Parzen window, we analyzed the effect of the ratio between the number of atlas bundle seeds and the number of subject bundle seeds. To do so, the data of an HCP subject was processed with the *TractoFlow* [53] pipeline and used for the subject seeds. We tested five subject/atlas bundle ratio values [0 : 1, 0.2 : 0.8, 0.5 : 0.5, 0.8 : 0.2, 1 : 0]. Following those ratios, rejection sampling was used to sample 30,000 new points over the empirically estimated PDF. Finally, after decoding those new latent points, we filtered according to the plausibility assessment criteria used in GESTA [31] for the length range, the WM coverage, the maximum curving angle, and the local streamline orientation to fODF peak angle (see appendix A.2 for more details). Fig. A.1a presents the latent space seed ratio values for 9 selected bundles – namely the AF_L, the AF_R, the PYT_L, the PYT_R, the CC_Pr_Po, the IFOF_L, the IFOF_R, the UF_L, and the UF_R –, in comparison with the final, post filtering steps in the FIESTA-gen filtering process, obtained WM volumes. Fig. A.1b shows the post-filtering FIESTA-gen streamline yield. A higher yield means that fewer streamlines are removed by all filtering steps in the FIESTA-gen filtering process. Overall, results suggest that a good trade-off ratio is 0.5:0.5, i.e., a latent space composed of 50% of streamlines from the subject bundle and 50% from the atlas bundle has a good yield rate with a high bundle volume. Thus, in this work, we adopted a subject-to-atlas seed ratio value of 0.5:0.5.

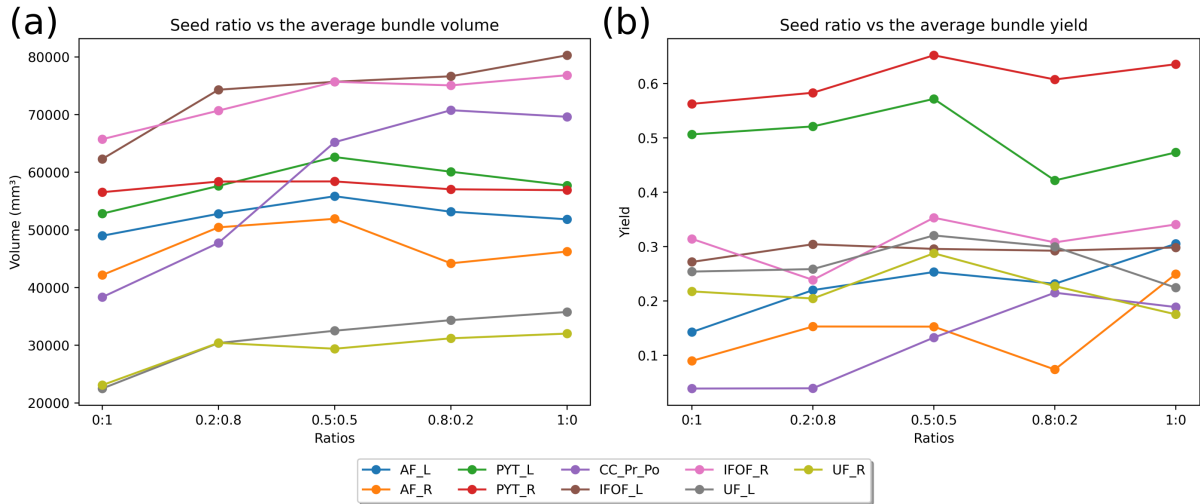


Figure A.1: (a) Volume over 9 selected bundles in the PAWM atlas resulting from the FIESTA-gen process with 30,000 streamlines sampled in the latent space followed by all the filtering steps in the FIESTA-gen filtering process. Thus, the final number of streamlines is variable and below 30,000. We hereby report volumes post-filtering. (b) Percentage of kept streamlines after the FIESTA-gen filtering process. The x-axis shows the composition of the latent space, with X:Y being the proportion of the subject bundle streamlines and the proportion of the atlas bundle streamlines.

A.4 Bundles compared across the 5 benchmark state-of-the-art methods

Table A.3: Bundles compared from each benchmarked method. Empty cells mean that the bundle was not defined by the method and was therefore ignored by subsequent computation

RB, RBx, FIESTA	TractSeg	WMA	XTRACT
AF_L	AF_left	T_AF_left	af_l
AF_R	AF_right	T_AF_right	af_r
CC_Oc	CC_7	T_CC7	-
CC_Pr_Po	CC_4	T_CC4	-
CG_L	CG_left	T_CB_left	cbd_l
CG_R	CG_right	T_CB_right	cbd_r
FPT_L	FPT_left	T_CR-F_left	-
FPT_R	FPT_right	T_CR-F_right	-
ICP_L	ICP_left	T_ICP_left	-
ICP_R	ICP_right	T_ICP_right	-
IFOF_L	IFO_left	T_IOFF_left	ifo_l
IFOF_R	IFO_right	T_IOFF_right	ifo_r
ILF_L	ILF_left	T_ILF_left	ilf_l
ILF_R	ILF_right	T_ILF_right	ilf_r
MCP	MCP	T_MCP	mcp
MdLF_L	MLF_left	T_MdLF_left	mdlf_l
MdLF_R	MLF_right	T_MdLF_right	mdlf_r
OR_ML_L	OR_left	T_SO_left	or_l
OR_ML_R	OR_right	T_SO_right	or_r
POPT_L	POPT_left	T_CR-P_left	-
POPT_R	POPT_right	T_CR-P_right	-
PYT_L	CST_left	T_CST_left	cst_l
PYT_R	CST_right	T_CST_right	cst_r
SCP_L	SCP_left	-	-
SCP_R	SCP_right	-	-
UF_L	UF_left	T_UF_left	uf_l
UF_R	UF_right	T_UF_right	uf_r

A.5 PAWM atlas

For the development and the evaluation of the current pipeline, we used a homemade and publicly available Population Average of WM (PAWM) atlas to evaluate our framework [54]. The PAWM atlas was built in the context of *RecoBundlesX* works by Rheault, F. *et al.*, (2020) [19, 20] based on ExTractor [55] and well curated by a neuroanatomist to finally have bundles that fit their normative shapes [54]. The PAWM atlas was created from 20 random UKBioBank [69] subjects' probabilistic tractograms (ensemble tractography from WM seeding and interface seeding with PFT tracking [9, 70]). Tractograms were filtered for implausible streamlines using ExTractor [55], and bundles of interest were extracted from sequences of anatomical rules applied only to anatomically plausible streamlines.

Nonlinear registration using cross-correlation metric between the subjects' T1w images and the MNI152 2009c Nonlinear Symmetric template was performed using Ants [71]. The affine transformation and deformation fields were applied to bundles, and visual quality control confirmed bundles were adequately reconstructed and warped to the template.

Matching bundles were merged to obtain a representative population average for each bundle. Bundles were then manually cleaned using a clustering approach. Bundles were decomposed into clusters using *QuickBundlesX* [16]. Each cluster was inspected and accepted or discarded to remove outliers (streamlines with aberrant shapes), incomplete streamlines, or extremely noisy clusters. This manual method allowed thorough filtering of implausible streamlines, while preserving sparse/rare, but anatomically valid, streamlines (e.g., fanning streamlines, streamlines in hard-to-track bundles).

The next step consisted of a symmetrization of both hemispheres. To avoid introducing a left/right bias in FIESTA's bundling step, the association and projection atlas bundles were mirrored across hemispheres. Using the spatial transformation of the MNI152 template, bundles were flipped on the X-axis and locally registered to their analogous bundles on the other side using a (constrained) rigid Streamlines Local Registration (SLR) [41]. This ensured a better final overlap that matched the expected position of each bundle.

Finally, all bundles were downsampled to a maximum of 10,000 streamlines to reduce computational burden. Streamlines were upsampled, smoothed using a 3D Gaussian kernel applied to the vertices along each streamline, and re-compressed [72]. This led to a final lightweight, population-averaged, anatomically meaningful atlas of WM bundles. Fig. 2 presents a representation of all the bundles in the PAWM atlas. The bundle full names, abbreviations, and labels used in this work are indicated in Table A.1.